ARMY RESEARCH LABORATORY

Temporal Behavior of Natural Terrain Radiance at Infrared Wavelengths

by Max P. Bleiweiss and Christopher D. Padilla
U.S. Army Research Laboratory
Battlefield Environment Directorate

ARL-TR-1017 December 1996

Approved for public release; distribution unlimited.

NOTICES

Disclaimers

The findings in this report are not to be construed as an official Department of the Army position, unless so designated by other authorized documents.

The citation of trade names and names of manufacturers in this report is not to be construed as official Government indorsement or approval of commercial products or services referenced herein.

Destruction Notice

When this document is no longer needed, destroy it by any method that will prevent disclosure of its contents or reconstruction of the document.

REPORT DOCUMENTATION PAGE

Form Approved
OMB No. 0704-0188

1. AGENCY USE ONLY (Leave blank)	2. REPORT DATE	3. REPORT TYPE AND DATES COVERED
	September 1996	Final

4. TITLE AND SUBTITLE
Temporal Behavior of Natural Terrain Radiance in Infrared Wavelengths

5. FUNDING NUMBERS

6. AUTHOR(S)
Max P. Bleiweiss and Christopher D. Padilla

7. PERFORMING ORGANIZATION NAME(S) AND ADDRESS(ES)
U.S. Army Research Laboratory
Battlefield Environment Directorate
Attn: BE
White Sands Missile Range, NM 88002-5501

8. PERFORMING ORGANIZATION REPORT NUMBER
ARL-TR-1017

9. SPONSORING/MONITORING AGENCY NAME(S) AND ADDRESS(ES)
U.S. Army Research Laboratory
2800 Powder Mill Road
Adelphi, MD 20783-1145

10. SPONSORING/MONITORING AGENCY REPORT NUMBER
ARL-TR-1017

11. SUPPLEMENTARY NOTES

12a. DISTRIBUTION/AVAILABILITY STATEMENT
Approved for public release; distribution unlimited.

12b. DISTRIBUTION CODE
A

AD A 320452

13. ABSTRACT *(Maximum 200 words)*

Because most infrared observation of natural terrain are made at infrequent or widely spaced time intervals, there is little information on the high time resolution variation in background radiance. This is in spite of the fact that meteorological and other influences can cause apparent radiance to change by amounts equivalent to a few degrees Kelvin in seconds or tens of seconds. Infrared imagery acquired during the recent Smart Weapons Operability Enhancement Joint Test and Evaluation allows the investigation of the nature of IR radiance fluctuations with high time resolution under a variety of dirunal and meteorological conditions. During the Grayling I deployment, images were acquired at a rate of 6.25 frames per second, for 10 s every five min during each of the 2 h mission periods. There were 107 mission periods during the 41-day test. A portion of these images have been segmented according to homogeneous features (determined independently of the image content) and histograms of apparent tempreature within those features have been processed to allow studies of the temporal variation of radiance. The nature of the fluctuations as a function of meterological, atmospheric, and diurnal conditions is discussed; however, the result of this study is that the range of variation within the 10 s period, for the missions studied, is very small. The largest range observed for any of the ROIs was 1 K.

14. SUBJECT TERMS	15. NUMBER OF PAGES
backgrounds, radiance, IR, time	83
	16. PRICE CODE

17. SECURITY CLASSIFICATION OF REPORT	18. SECURITY CLASSIFICATION OF THIS PAGE	19. SECURITY CLASSIFICATION OF ABSTRACT	20. LIMITATION OF ABSTRACT
Unclassified	Unclassified	Unclassified	SAR

Preface

Because most infrared observations of natural terrain are made at infrequent, or widely spaced time intervals, information on the high time resolution variation in background radiance is lacking. Meteorological and other influences can cause apparent radiance to change by amounts equivalent of a few degrees Kelvin in seconds or tens-of-seconds. Most summaries of scene statistics consider only spatial components. Attempts to assemble statistics of the temporal component of scene variability are non-existent. The phenomenon considered here is not the well known situation of a partly cloudy sky that causes variation in radiance due to shadows, although this can be a factor. For example, while supporting a U.S. Army smoke test in the late Spring of 1989, observations showed wide variation in infrared background radiance (figure 1). The existence of such phenomena indicates that false targets can come and go in imagery, which may replicate the appearance of real targets. This observation resulted in an extensive literature search to determine if similar observations had been made, if there are existing databases that might be examined for such phenomena, and if the existence of such phenomena had been hypothesized and/or explained. We concluded that there were no known similar observations, or databases containing data capable of yielding similar observations.

Infrared imagery acquired during the Grayling I field exercise of the SWOE JT&E were processed to investigate characteristics of the temporal variability in radiance of individual scene elements. The lack of continuous imagery for long periods limited the scope of this study. Instead of studying the apparent radiance over continuous periods, 10-s periods (sampled at 6.25 Hz) were segmented from the data set and one period for each of the mid- and far-infrared wave bands was processed from each of 40 different mission periods . The 12, 10-s periods for 3, 1-h mission periods were also processed (1, 10-s period every 5 min). This allowed the investigation of the variation during a 1-h period. The results of the 40 mission periods showed that the variation observed, during a 10-s period, was of the instrumental noise. The largest variation observed during any 10-s period was 1 Kelvin. This could be a significant result when the observations are compared to typical background scenes with targets. However, that determination will be left

to a later study. The investigation of the three, 1-h periods seems to indicate that the variability is more closely tied to wind speed than other meteorological factors, and the vegetation elements seem to show more variability than the ground elements.

Future work should be directed towards the study of the additional SWOE data as well as the data acquired over the years at WSMR. This latter data set consists of observations made at WSMR for which there is also a complete set of meteorological data acquired at 1-s intervals during the observations and at 15-min intervals during non-observation periods during the last five years. The SWOE data should be first investigated in a similar manner for the Yuma I field exercise and then the contiuous, high-time resolution data should be analyzed from both Yuma I and Grayling II.

Contents

Figures

Tables

Acknowledgment

This effort was partly funded through funds provided by the Smart Weapons Operability Enhancement Joint Test and Evaluation office, J.P. Welsh, Director.

1. Executive Summary

In the Spring of 1989, infrared (IR) observations were made at the north end of the White Sands Missile Range (WSMR) as part of test support for an Army system. Observations showed that unusual temporal variations in the radiance of some background scene elements occurred. These variations occurred over time scales of a few seconds to tens-of-seconds with an amplitude of a few degree Celsius (C) in apparent temperature. Correlative measurements could not explain what was happening, except to confirm that the radiance was changing. The variation could not be ascribed to either variation in atmospheric transmittance or other phenomena, including instrumental effects. A literature search found little or no remarks concerning such phenomena. There are no known databases of IR backgrounds that could be studied for such a phenomena. An in-depth study of a local portion of the main post area at WSMR was conducted. The scene was characterized and meteorological stations were set up; the scene was monitored with IR and visible imagers on a semi-regular schedule for several years. However, limited resources and pressing commitments have not allowed much analyses to proceed with the data. The advent of the Smart Weapons Operability Enhancement (SWOE) Joint Test and Evaluation (JT&E) Program allowed the collection of IR images of natural background scenes, but the temporal resolution was not as continuous or as frequent as desired. The data was in a digital format and more amenable to analyses than the hours of videotape of the local study area at WSMR. To establish a methodology for analyses, and to begin the study of the temporal variation of natural background scene radiance with high time resolution, selected portions of the SWOE JT&E data were processed. This report describes the study and presents the results.

The SWOE data used in this study consists of two sets taken from the Grayling I field test. The first set consists of IR images collected during the first 10-s period from each of the 40 critical missions (missions chosen for comparison of real and synthetic imagery). The second set consists of IR images collected during the first 12, 10-s periods from three other missions. For the data studied here, each mission consisted of a 2-h, data-collection period with 10 s observations every 5 min . IR images were used, of a natural background scene collected at a rate of 6.25 frames

per second (FPS). Each image was segmented into eight regions of interest (ROIs) for further analyses. The average apparent temperature for each sample was determined for each ROI. Time-averaged region temperatures and range of temperature variation for the 10-s period were also determined. The latter values are used in this study.

The range of variation within the 10-s period, for the 40 missions studied, was very small. The largest range observed for any of the ROIs was 1 Kelvin (K). The bulk of the ranges fell at the noise level of the instruments, "the noise equivalent temperature difference (NETD) for the imagers is 0.3 K and 0.1 K for the mid- and far-IR, respectively." [1]

An attempt at exploratory data analyses was made to see if a relationship existed between the observed meteorological conditions and the ranges of apparent temperature within the ROIs by plotting the meteorological parameters (wind speed, visibility, air temperature, relative humidity, global flux, and time of day) versus the range. Global flux was the only trend, and it showed a small relationship. No attempt was made for a proper comparison because of the probable lack of meeting the assumptions required for correct statistical analyses.

The three mission periods from the second data set showed distinct differences over the 1-h period. However, the data also shows the same results as the study of the first 10-s periods. The longer length of time allowed the appearance of trends, but the lack of continuous observation precluded any efforts beyond the above results with ranges in the averages of the 10-s periods during the hour (by ROI).

The phenomenon seen in the WSMR data, not replicated in the Grayling data, was climate. The meteorological aspects of the climatological differences as well as the vegetative differences between Grayling and WSMR should be studied.

1. Introduction

Information on the high-resolution time variation in background radiance is lacking because most IR observations of natural terrain are made at erratic time intervals. Meteorological and other influences also cause apparent radiance to change by amounts equivalent to a few degrees K in seconds or tens-of- seconds. Most summaries of scene statistics consider only the spatial component. No attempt has been made to assemble statistics of the temporal component of scene variability. The phenomenon we considered was not that of a partly cloudy sky causing variation in radiance due to shadows; although, this can be a factor. For example, while supporting a U.S. Army Smoke Test in the late Spring of 1989, observations showed wide variation in IR background radiance (figure 1). The significance of this phenomena is that false targets can come and go in IR imagery, replicating the appearance of real targets. Meteorological and other pertinent conditions when these observations were made include:

- high elevation (7000 ft above sea level) in southern New Mexico assumes that the ambient atmospheric influences on attenuation, etc. would be minimal;

- noon time, so a period of slow change is expected. The diurnal variation of apparent temperature shows maximum change during late morning and late evening, with a peak in early afternoon and a minimum in early morning; depending on the particular scene element and the optical and thermal properties, these phenomena may change accordingly;

- benign meteorological conditions, such as clear sky (no clouds whatsoever), relatively calm wind conditions, and low relative humidity;

- many collateral measurements, including variations seen in only part of the image (equipment problems can be ruled out); when the disturbance was localized and moved across the field of view of the imager; transmission measurements along the same line of sight (no variation observed in either visible or IR bands); and visible color and black and white video observations

along the same lines of sight (no obvious variation in the scene; for example, no dust clouds observed, etc.).

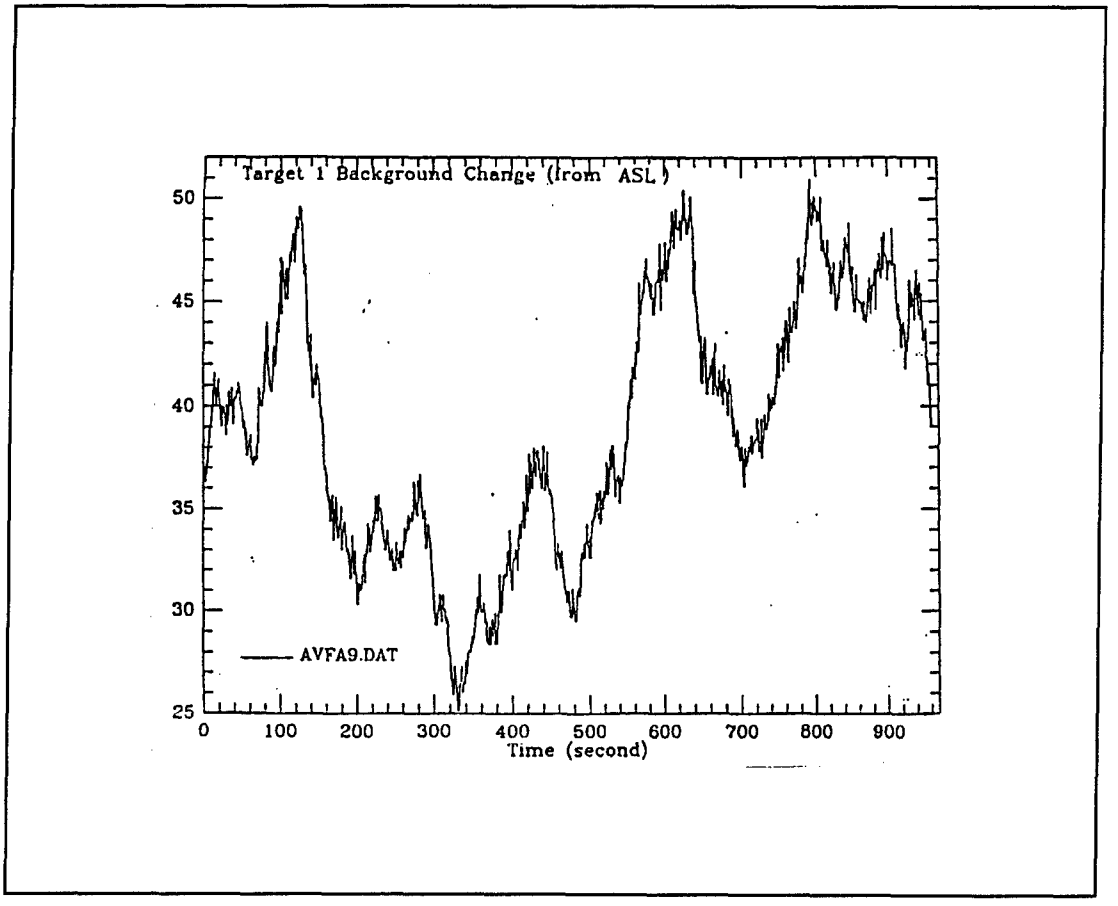

Figure 1. An example of the large and rapid variation of IR background radiance. The amplitude scale is in units of an 8-bit gray scale; the range of 256 units is scaled to an approximate 20-K range of apparent temperature, 10 units is approximately 0.8 K. This can be related to radiance because the temperature would be measured if the equivalent amount of radiance were due to a blackbody at that temperature.

This observation triggered an extensive literature search to determine if similar observations had been made, if there were existing databases that might be explored for such phenomena, or if the existence of such phenomena had been hypothesized and/or explained. The outcome of this search culminated in a report by New Mexico State University's (NMSU) Physical Science Laboratory. [2] The results determined that no similar observations or existing databases (such as those

at the Environmental Research Institute of Michigan, [3] and Eglin Air Force Base's Target and Background Information Library System [4]), contained similar data. Existing theory [5] can explain these observations through known processes. For example, phenomena with variation in emissivity can be caused by the wind blowing leaves on a bush, or a variation in transpiration of vegetation. The definitive cause for the variations shown in figure 1 remains to be discovered because of a lack of complete information at the time the observations were made.

An extensive observational program of local terrain at WSMR was instituted to investigate the phenomena in detail. Due to reorientation of effort and reduction of resources, the data remains to be reduced and analyzed. Instead, recently acquired data (in a more amenable format) was used for the current investigation. IR imagery, both mid-IR (3 to 5μm) and far-IR (8 to 12μm) bandpass acquired during the recent SWOE JT&E (though not obtained for long periods with high-time resolution) was in digital format and existed for short periods with high-time resolution and provided data to begin a study. Specifically, during the Grayling I deployment, images were acquired at the rate of 6.25 FPS, for 10 s every 5 min during each of the 2-h mission periods. The range to the mid-point of the scene was about 150 m, so with the nominal 20° FOV lenses, the spatial resolution was about .4 m. There were 107 mission periods during the 41 days of the test.

Of the 107 missions, a smaller subset of observation periods was selected. A smaller subset of images had been previously registered to the scene. An ROI segmented from an image obtained during one mission, can be assured of coming from the same portion of the scene for another mission. For example, a given ROI always samples the exact same scene element (tree, ground, etc.). Registration procedures were required because the look angle of the imagers was not always exactly the same, mission to mission; it caused small variations of the resultant FOV of the imager, and resulted in small differences between ROIs from one mission to another. This resulted in inconsistent comparisons between missions. The details of the image registration process can be found in the SWOE JT&E final report. [6]

Two divisions of the data were made for the missions. The first mission was to download the first 10-s period from each of the missions, resulting in 60 images per mission over a 10-s period, available for further study. The other set was taken from the first hour of three mission periods, spanning a wide range in diurnal conditions. This later set consisted of 12, 10-s periods to obtain some idea of variation over a 1-h period. This data set was a very limited subset of the total set obtained during the SWOE JT&E. Although not the best for this study, it was the most accessible. There were times during the other two SWOE field exercises when data collection was more extensive. For example, during Yuma I, there was a 24-h period when one image was acquired each second. During Grayling II (during the non-mission periods) an image was acquired every 15 s for 40 days. Attempts will be made to access this data at a later date. The images studied here were segmented according to homogeneous features determined independently of the image content. Figure 2 shows an image with the ROIs indicated by boxes drawn on the sample image. Histograms of apparent temperature within those features were formed for further analyses.

The following discussion begins with a brief review of radiative heat transfer as it applies to the problem under study. Next, the details of the data reduction based on these histograms is presented. A discussion follows on the nature of the fluctuations as a function of meteorological, atmospheric, and diurnal conditions.

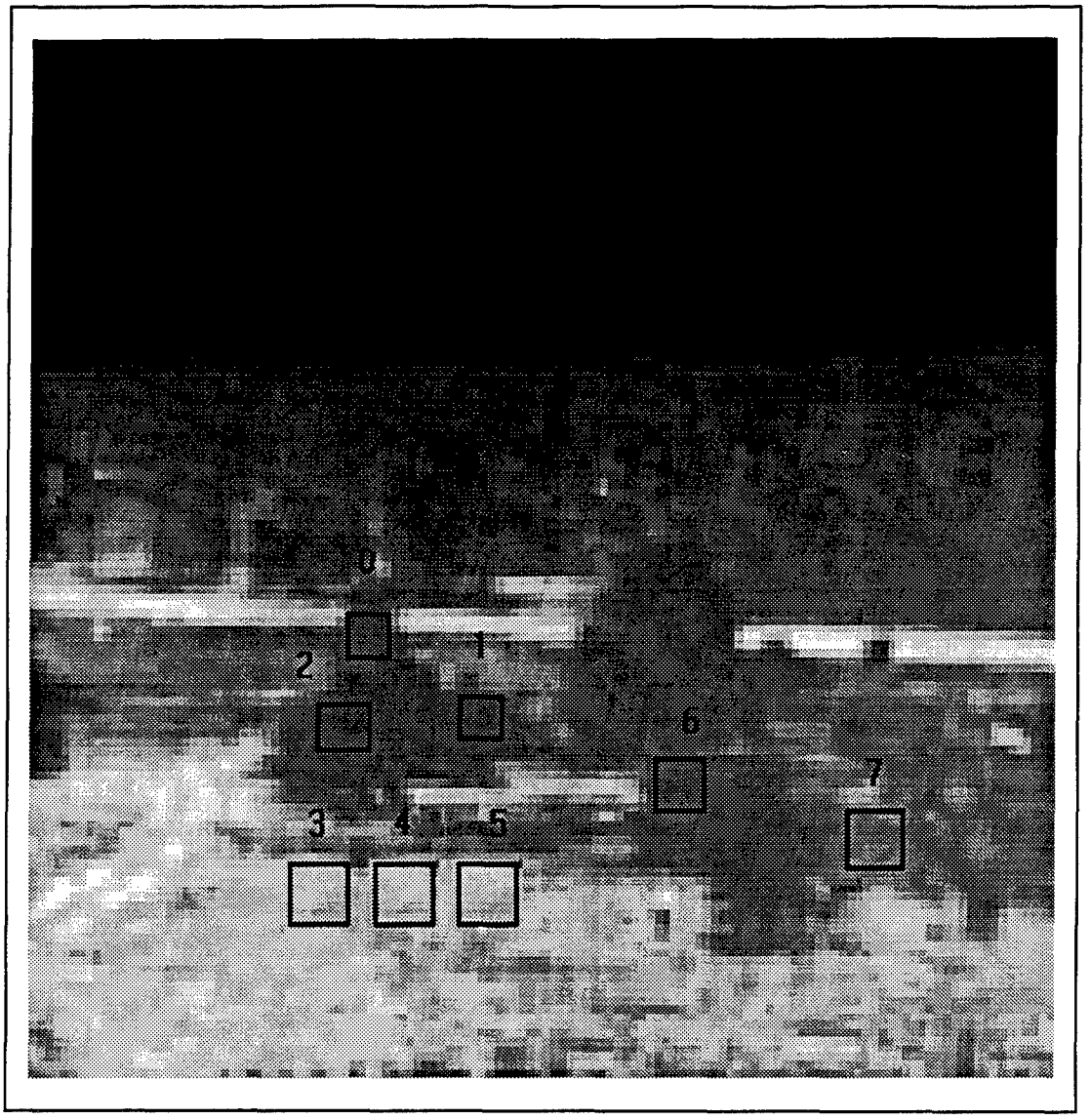

Figure 2. An example of the type of image; notation shows the position of the ROIs.

2. Literature Review

Ben-Yosef and Wilner and Ben-Yosef et al. investigated the daily variation of IR radiance statistics. [7] [8] They were interested in how the statistics of radiance in an image varied with spatial and temporal resolution. They concluded that there are increases in contrast within an image during transient heating and cooling. Under these conditions, the contrast would be larger than that experienced during steady-state conditions. In the first case, while the observations had high temporal resolution, the experiment was conducted under controlled conditions, so the type of phenomena witnessed could be observed. Ben-Yosef and Wilner confirmed that different objects in a scene heat and cool at different rates; during transient events some scene elements experience more variability than others. In the latter case, the emphasis was on natural scene statistics derived from an imager. Their observations, covering only a portion of the diurnal cycle, appear to be at about 30-min intervals and did not yield the same sort of phenomena investigated here. Depending on the thermal inertia of the scene element and time of day, relatively rapid changes could occur. [9]

Ben-Yosef et al. report the time constants in the heat balance equation are 1000 s during very benign environmental conditions, and for instances of a scene composed of components, not prone to variability. [10] Their work modeling the radiation statistics does not consider the rapid fluctuations possible in an environment with much variety.

The energy budget under consideration concerns both living organisms (vegetation) and non-vegetative materials (dirt, rocks, sand, etc.). The energy balance equation is:

$$M+Q_a=R+C+\lambda E+G+X \qquad (1)$$

where

M = rate metabolic energy is generated
Q_a = amount of radiation absorbed by the surface of the organism
R = radiation emitted by the surface of the organism
C = energy transferred by convection
λE = energy exchanged by evaporation or condensation of moisture
G = energy exchanged by conduction
X = energy put into or taken out of storage within an organism. [5]

Consideration of the equation is beyond the scope of this paper; however, it is included to place the phenomena into perspective. Each of these terms is a complex variable in time and whose dependence on thermal and optical properties can also be temporally variable. For vegetative cover, these variables depend on such things as leaf size, type of organism (desert plants behave differently than plants native to other climates, plants will have leaf temperatures below or above air temperature, etc.), wind speed, relative humidity, and so on. The phenomena that instigated this study was probably the result of either a variation of transpiration of the vegetative cover of the scene under observation, or a variation in optical properties (such as emissivity); both could have been caused by wind-speed variation.

Gates reports instances of leaf temperature changes occurring over a period of 6 s, by 7° to 10° C, due to no cloud/cloud variations and leaf temperature changes occurring instantaneously; by 10 °C, due to changes in wind/no wind, [5] which confirms the above presumption, and could lead to instances where an isolated cluster of vegetation (bushes) could appear as a target. If a gust moved across a vegetated field then a target could also appear to move. Investigating these types of phenomena requires temporal resolution on the order of fractions of a second, using relatively wide-angle FOV imagery. The SWOE JT&E database allows such a study for short periods.

3. Data Reduction

The images of the scene were segmented to allow the investigation of the temporal evolution of individual scene elements such as localized, homogeneous portions of the image (trees, bushes, and ground). Some of the scene elements were duplicated to discover if the elements thought to be homogeneous were, and if they would respond to the same stimulus. This resulted in eight ROIs of varying square dimensions, used to form histograms of the pixel-apparent temperature. Figure 2 shows the location of the ROIs. Table 1 lists the characteristics of the ROIs. ROI 0, 1 2, and 6 were chosen to determine variation between like kinds of vegetation. ROI 3 through 5 were chosen to allow replication of the sampling (all three were relatively close to one another and covered identical patches of ground), and ROI 7, though thought to represent the same type of scene element as ROIs 3 through 5, appears to have a different apparent temperature and might represent a different type of scene element.

Table 1. ROI characteristics

Region number	Region size, pixels	Scene element type
ROI 0	3 by 3	coniferous tree
ROI 1	3 by 3	coniferous tree
ROI 2	4 by 4	coniferous tree
ROI 3	8 by 8	sparse grass
ROI 4	8 by 8	sparse grass
ROI 5	8 by 8	sparse grass
ROI 6	6 by 6	coniferous tree
ROI 7	8 by 8	sparse grass

Initially, the plan was to determine a variety of first order statistics based on the histograms of the apparent temperature within the ROI, and to observe the temporal evolution of these parameters. This was accomplished; however, the variability of these parameters was so small that it was difficult to arrive at any conclusions. The next step was to determine the range of the integrated (weighted) apparent temperature. The range (the difference between the maximum

and minimum value) of the average within the ROI was determined and studied. The reason for the change in terminology is that "comparison of means," as implied by the determination of the range of means or averages, could only be effected if the distributions under study are normal distributions. We did not think it was profitable to make this determination. Instead, we used the average weighted integral, which is very similar to, or nearly proportional to what would be observed if the instantaneous FOV of the instrument were the same as the ROI in size and had a "point response function" that could be emulated by a rectangular response function. The data we considered was the set of 10-s observations from the beginning of each of the 40 mission periods, for each waveband. The results of this data reduction are presented in Appendix A, which contains the plots of the distribution of ranges by ROI and waveband for each of the 10-s periods. Table 1 shows that the number of pixels forming the average is varied, depending on the size of the ROI (9, 16, 36, or 64 pixels).

For the 1-h data sets, the results from the 12, 10-s periods were similar to that obtained for the one, 10-s period discussed above. Thus data was processed to determine the weighted, integrated (average) apparent temperature for each of the 10-s periods, to determine the average and range of that parameter over the 10-s period, and to plot these quantities as a function of time. The results of this processing appear in Appendix B, where plots are presented for each of the three missions and both wavebands. It is understood that the proper way to sample a time series is to observe at a rate at least twice the Nyquist frequency for a band-limited signal. In our case, that was impossible (we cannot band-limit nature); we took samples at a rate at least twice as fast as the expected, or known variation, in the background radiance. Until we know more about this phenomena, we cannot sample at a very high rate for long periods because of the limitations of available resources and the inability to reduce such large amounts of data. This first attempt at analyses was to make an initial investigation for developing a methodology.

Also, for the 3, 1-h periods, the range of the integrated value during the 10-s period was plotted with time (by IR-bandpass and mission period). The results appear in Appendix C. Appendix D contains the air temperature, downwelling

precision spectral pyranometer (PSP) radiation, and 2-m wind speed at 1-min intervals, plotted for each of the 3, 1-h periods.

4. Results and Discussion

The range of variation within the 10-s period for the 40 missions studied was very small. The largest range observed for any of the ROIs was 1 K. The bulk of the ranges fell at the noise level of the instruments. [1] The NETD for the imagers was 0.3 K for the mid-IR and 0.1 K for the far-IR. This can be seen by inspecting the histograms of range, by ROI and waveband. For the mid-IR band, the histograms show a maximum at 0.2 or 0.3 K, with a tail out to a maximum range of 0.5 K. The far-IR band peaks at 0.1 K and has a maximum range of 1 K. The results indicate that the mid-IR is marginally more temporally variable than the far-IR. The result is not unexpected; the mid-IR is more susceptible to variations in scattering of available radiation than is the far-IR. However, the results can be confused by the more noisy mid-IR system. In any case, the variation is small. Whether or not it is insignificant remains to be determined when the results are compared to target/background differences.

An attempt at exploratory data analyses was made to see if there might be some relationship between the observed meteorological conditions and the ranges of apparent temperature within the ROIs. Scatterplots created using the meteorological parameters (wind speed, visibility, air temperature, relative humidity, global flux, and time of day) versus the range (with the exception of the global flux, which showed a small relationship), showed no obvious trends. There was no attempt to make a proper comparison because of the probable lack of meeting the assumptions required for correct statistical analyses.

The three mission periods examined show distinct differences over the 1-h period studied. Mission 17 exhibited a trend during the period where the 10-s average changed by nearly 4 K from start to end, with variation between 10-s periods as large as about 0.8 K. Mission 40 began with an average apparent temperature 0.5 K higher than the hourly average, reaching a minimum of about 0.4 K below the average at 30 min into the hour, and increasing again near the end of the hour. The trends during Mission 48 showed almost no variation in the average apparent temperature (10-s average) from 1, 5-min period to the next, except near the end of the period when slight increases were noted. ROI 0, 1, and 2 showed less of an

increase than the rest. Local time for the three mission periods were, 1100, 2300, and 0700, respectively; the trends over the 1-h periods could be attributed to the variation in, or lack of solar radiation. The wind speed was nominally 3.5, 1.5, and 0 m/s during the periods, and might explain the period-to-period variation in averages; it was greatest for missions 17 and 40, and least for mission 48. There were some variations between the mid-IR and far-IR. For example, as the sun rose during mission 48, the mid-IR seemed to increase by larger amounts and the ground increased more than did the vegetation for the period-to-period changes in average values. The range of variation during the 10-s period for mission 48 showed almost constant variation with the mid-IR having ranges of 0.15 to 0.4 K, depending on scene element (the vegetation showed greater variation). The far-IR was also constant with ranges of about 0.05 to 0.1 K, with the vegetation only slightly more variable. Table 2 summarizes some of the observations, including the average apparent temperature experienced during the 1-h period and the range in the averages (by ROI) of the 10-s periods during the hour.

Table 2. Summary of the results of the 1-hr mission periods

Region	Mission 17 mid-IR		Mission 17 far-IR		Mission 40 mid-IR		Mission 40 far-IR		Mission 48 mid-IR		Mission 48 far-IR	
	Average	Range	Average	Range	Average	Range	Average	Range	Average	Range	Average	Range
ROI 0	289.91	1.34	287.63	1.65	287.64	0.62	285.63	0.81	275.16	0.50	272.03	0.19
ROI 1	290.09	1.65	288.01	1.82	287.47	0.55	285.29	0.71	275.10	0.54	271.89	0.28
ROI 2	290.03	1.65	287.99	1.76	287.47	0.63	285.35	0.81	275.15	0.50	272.04	0.23
ROI 3	295.32	3.27	291.85	3.43	285.21	0.85	281.92	1.15	274.31	0.90	271.00	0.83
ROI 4	294.82	3.08	291.66	3.37	285.26	0.94	282.25	1.08	274.22	0.86	270.93	0.81
ROI 5	295.14	3.32	292.23	3.62	285.16	0.76	281.92	0.92	274.40	0.84	270.96	0.82
ROI 6	290.19	1.73	287.96	2.04	287.15	0.62	284.83	0.77	275.04	0.49	271.81	0.40
ROI 7	294.33	1.53	290.43	2.27	285.43	0.67	282.00	0.94	273.89	1.05	269.85	0.93

No noted observations approached the variability seen in the WSMR observations. It may be that those observations were associated with phenomena not experienced during the Grayling Field Test. The data from the SWOE exercise has not been fully explored; the phenomena such as the WSMR results may be hidden there. More importantly, a technical reviewer pointed out the considerable climatological difference between Grayling and WSMR, a possible explanation for only small variations in apparent temperature being observed. [11]

Oke notes the difference between the energy balance for crops in a European climate (similar to the climate in Grayling) and a desert climate. [12] Besides the importance of the meteorological differences, the differences in the native vegetation is considerable. Deciduous desert plants have smaller leaves which orient themselves in a vertical direction. [5] Reorientation by wind could cause an increase in real and apparent temperature, as well as variation in reflective properties. [13] A meteorological explanation for the localized change seen in the WSMR data could be attributed to a whirlwind moving across the FOV. It would not have been visible if it did not carry dust with it. The convective conditions necessary for the formation of the whirlwinds are more common in desert climates than the temperate conditions experienced in Grayling. [12]

5. Summary and Conclusions

IR imagery acquired during the Grayling I field exercise of the SWOE JT&E was processed to investigate characteristics of the temporal variability in radiance of individual scene elements. The lack of continuous imagery for long periods limited the scope of this study. Instead of studying the apparent radiance over continuous periods, 10-s periods (sampled at 6.25 Hz) were segmented from the data set; one period was processed from each of 40 different mission periods for each of the mid- and far-IR wave bands. The 12, 10-s periods for 3, 1-h mission periods were also processed (1, 10 s period every 5 min). This allowed the investigation of the variation during a 1-h period. During a 10- s period, the results of the 40 mission periods showed that the variation observed was of the instrumental noise. The largest variation observed during any of the 10-s periods was 1 K. This may be a significant result when these observations are compared to typical background scenes with targets. However, that determination will be left for a later study. The investigation of the 3, 1-h periods seems to indicate that the variability is more closely tied to wind speed than other meteorological factors, and the vegetation elements seem to show more variability than do the ground elements.

Future work should be directed towards the study of the additional SWOE data as well as the data acquired over the years at WSMR. The WSMR data set consists of observations where meteorological data was acquired at 1-s intervals, and at 15-min intervals during non-observation periods during the last five years. Further study of the SWOE data should begin with a similar study of the Yuma I field exercise; then the continuous, high-time resolution data from both Yuma I and Grayling II should be analyzed.

References

1. Berger, R.H., and M.P. Bleiweiss, "Comparison of infrared radiometers used to gather background signature data," SPIE International Symposium on Aerospace/Defense Sensing and Controls, Orlando, FL, 1994.

2. Nolen, B., and D.D. Bustamante, "A review of thermal models and site data for the high temporal resolution characterization of natural terrain radiance fluctuations at the MIDAS/ATLAS site," PSL-91/46, Physical Science Laboratory, New Mexico State University, Las Cruces, NM, 1991.

3. Larocca, A.J., private communication, 1990.

4. Simpson, V., private communication, 1990.

5. Gates, D.M., *Biophysical Ecology*, Springer-Verlag, New York, 1980.

6. Bleiweiss, et al., "Appendix E: Analysis of the imagery and environmental data" in the"Final Report for the SWOE JT&E," J.P. Welsh, et al, U.S. Army Cold Regions Research and Engineering Laboratory, Hanover, NH, 1995.

7. Ben-Yosef, N. and K. Wilner, "Temporal behavior of thermal images," *Applied Optics*, **24**, 2, p. 284-286, 1985.

8. Ben-Yosef, N., K. Wilner, I. Fuchs, S. Simhony, and M. Abitbol, "Natural terrain infrared radiance statistics: daily variation," *Applied Optics*, **24**, 23, p.4167-4171, 1985.

9. Watson, K., "Geologic Applications of Thermal Infrared Images," *Proceedings of the IEEE*, **63**, Jan., p.128-137, 1975.

10. Ben-Yosef, N., K. Wilner, and M. Abitbol, "Measurement and modeling of natural desert terrain in the infrared," *Optical Engineering*, **27**, 11, p.928-932, 1988.

11. Tofsted, D.H., private communication, 1996

12. Oke, T.R., *Boundary Layer Climates*, Methuen & Co Ltd, London, 1978.

13. Vanderbilt, V.C., S.L. Ustin, and J. Clark, "Canopy geometry changes due to wind cause red edge spectral shift," Proceedings of IGARSS '88 Symposium, ESA SP-284 (IEEE 88CH2497-6) ESA Publications Division, 1988.

Acronyms and Abbreviations

C	Celsius
FPS	frame per second
FOV	field of view
IR	infrared
JT &E	Joint Test and Evaluation
K	Kelvin
NETD	noise equivalent temperature difference
NMSU	New Mexico State University
PSP	precision spectral pyranometer
ROI	regions of interest
SWOE	Smart Weapons Operability Enhancement
WSMR	White Sands Missile Range

Appendix A

Histograms of the Range of Weighted, Integrated, Apparent Temperature, for Each ROI (by waveband)

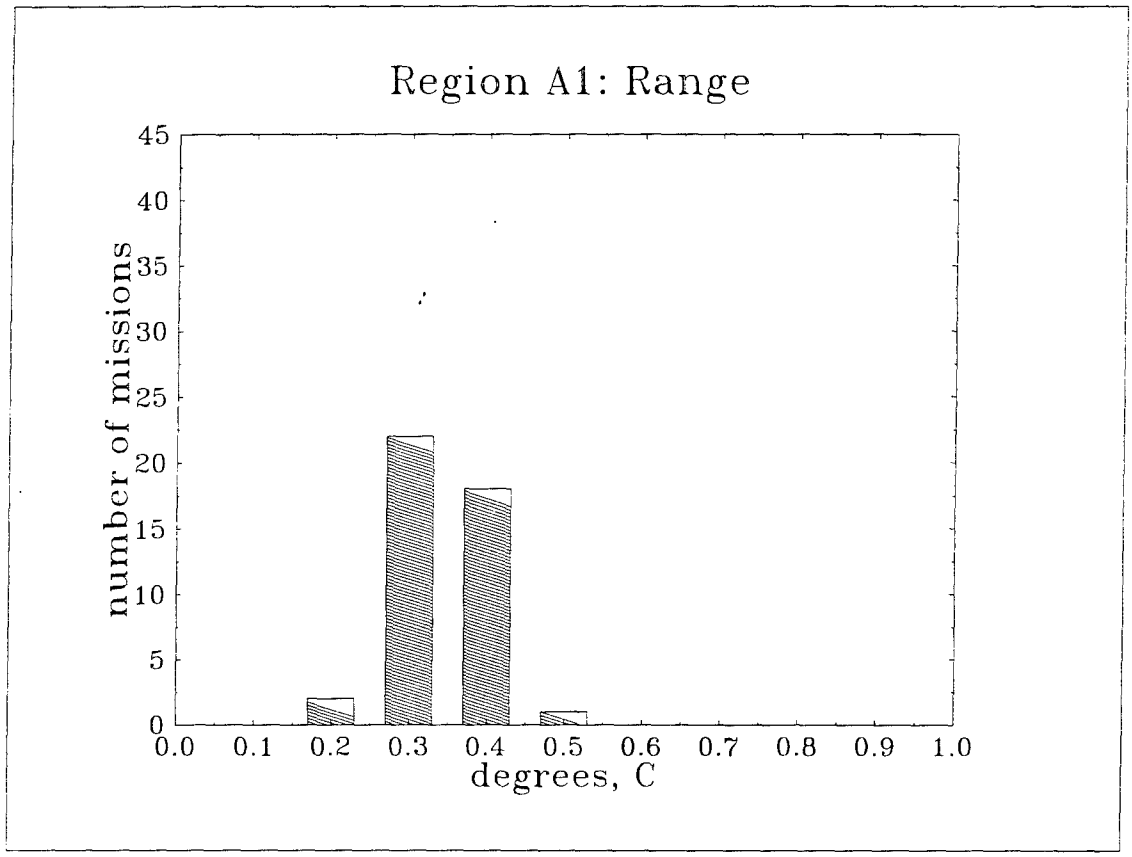

Figure A-1. Histogram of ranges of weighted, integrated apparent temperature experienced for each of the 10-s periods for the missions studied. This graph is for the mid-IR, ROI 0.

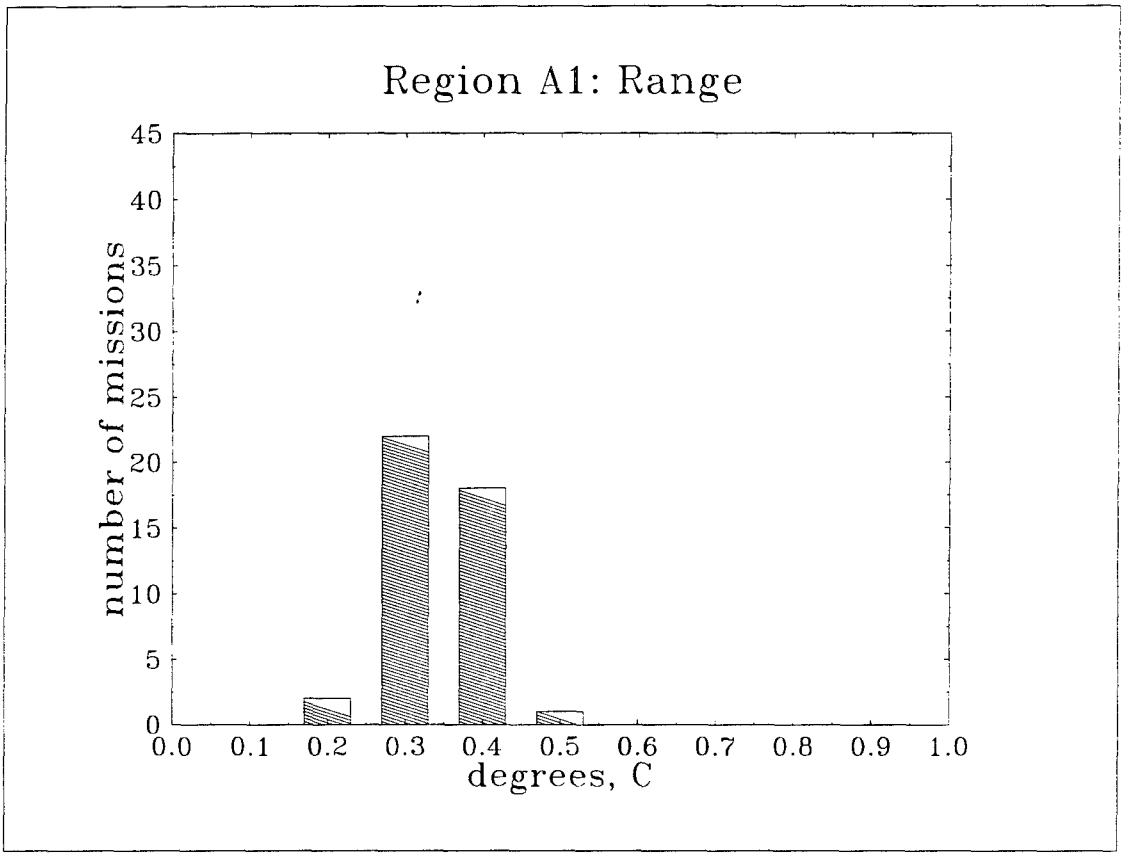

Figure A-2. Histogram of ranges of weighted, integrated apparent temperature experienced for each of the 10-s periods for the missions studied. This graph is for the mid-IR, ROI 1.

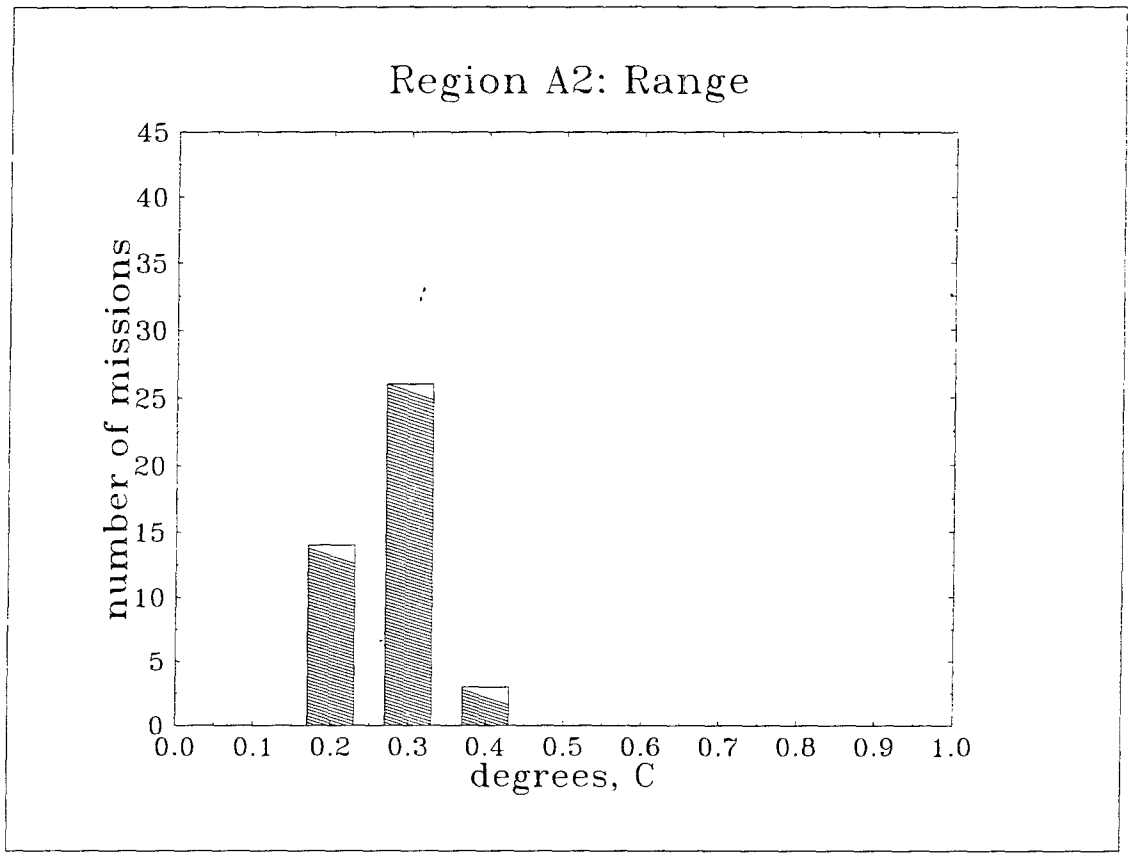

Figure A-3. Histogram of ranges of weighted, integrated apparent temperature experienced for each of the 10-s periods for the missions studied. This graph is for the mid-IR, ROI 2.

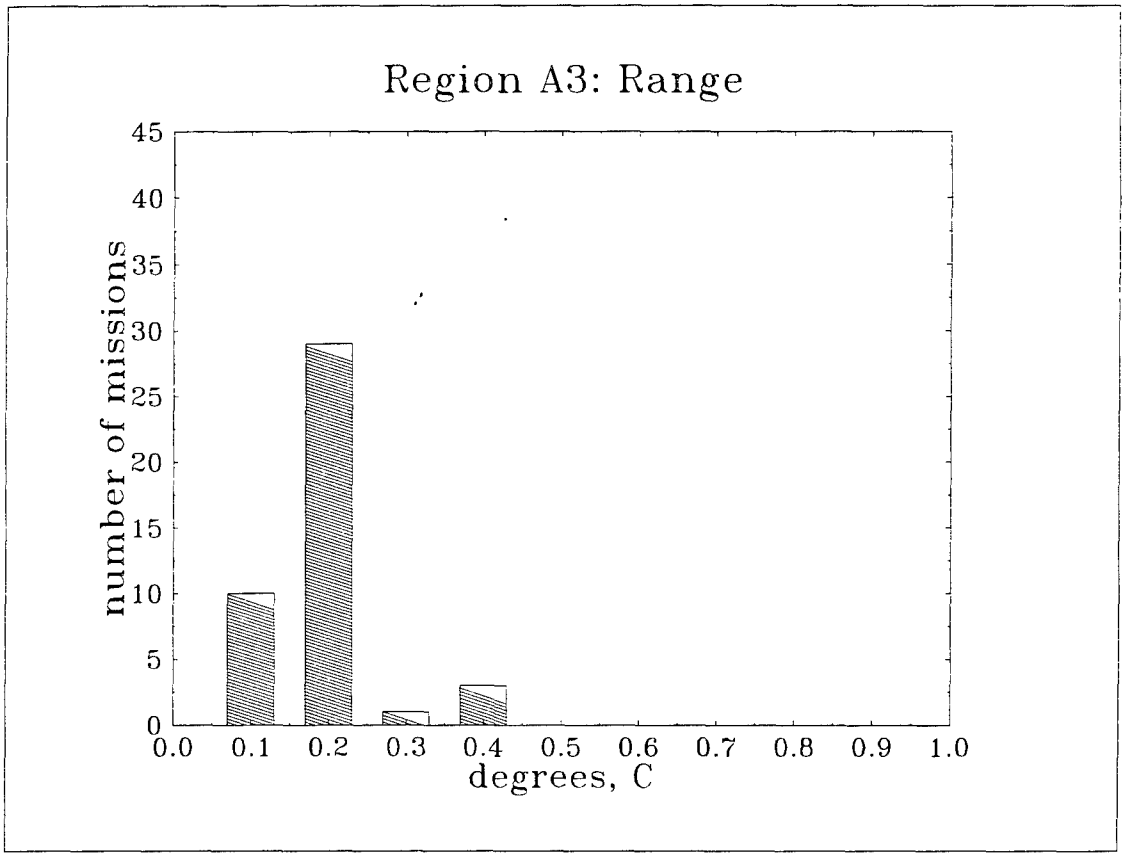

Figure A-4. Histogram of ranges of weighted, integrated apparent temperature experienced for each of the 10-s periods for the missions studied. This graph is for the mid-IR, ROI 3.

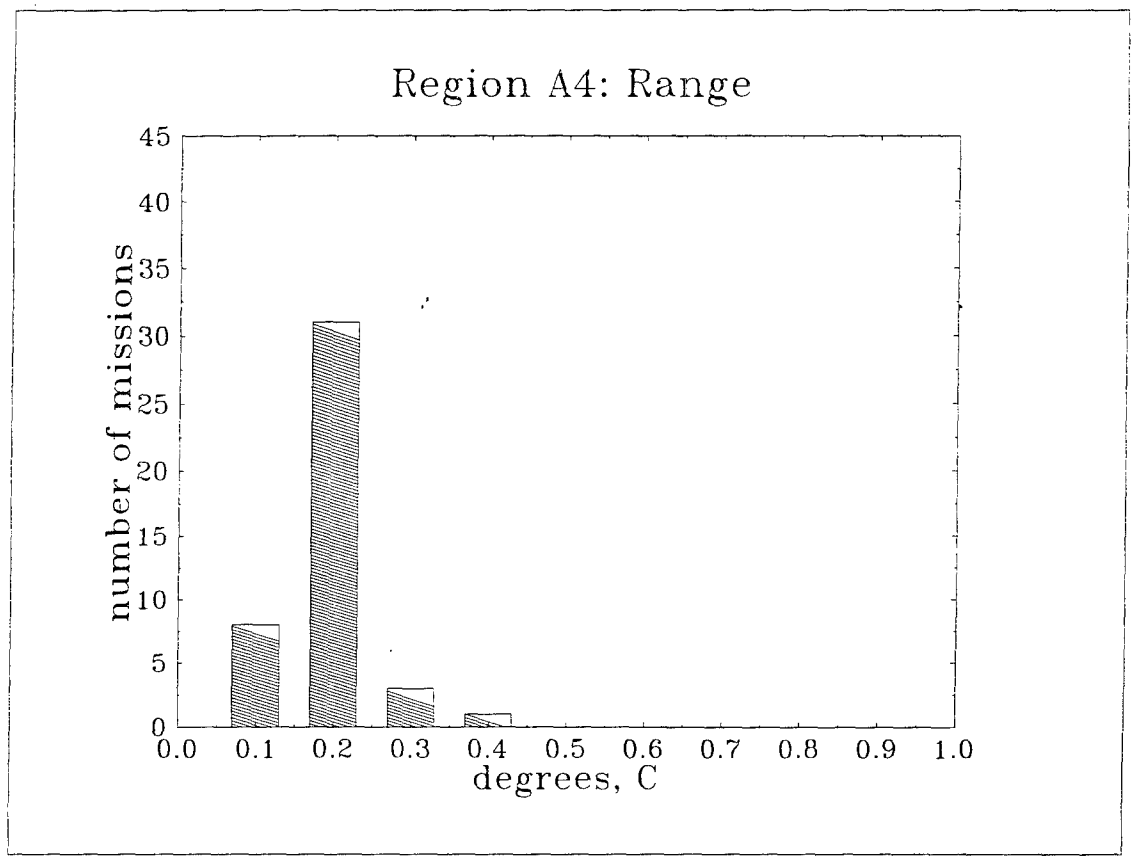

Figure A-5. Histogram of ranges of weighted, integrated apparent temperature experienced for each of the 10-s periods for the missions studied. This graph is for the mid-IR, ROI 4.

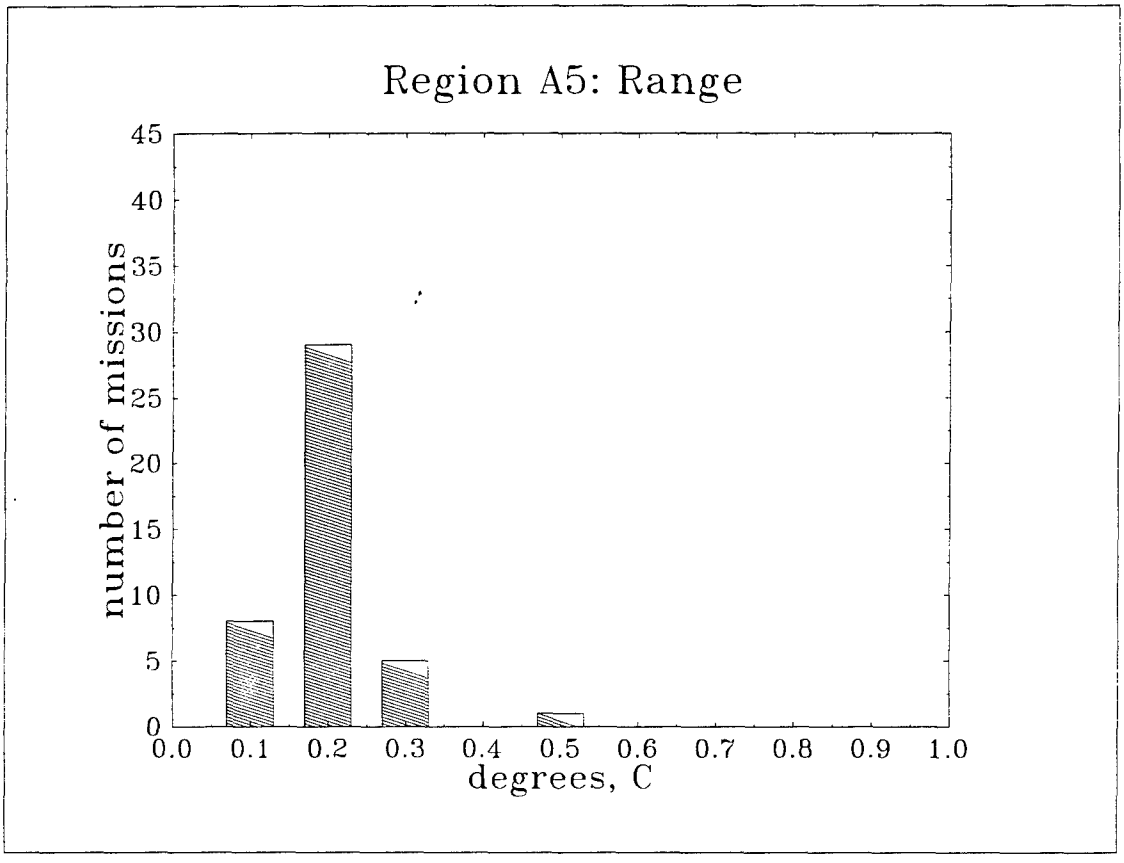

Figure A-6. Histogram of ranges of weighted, integrated apparent temperature experienced for each of the 10-s periods for the missions studied. This graph is for the mid-IR ROI 5.

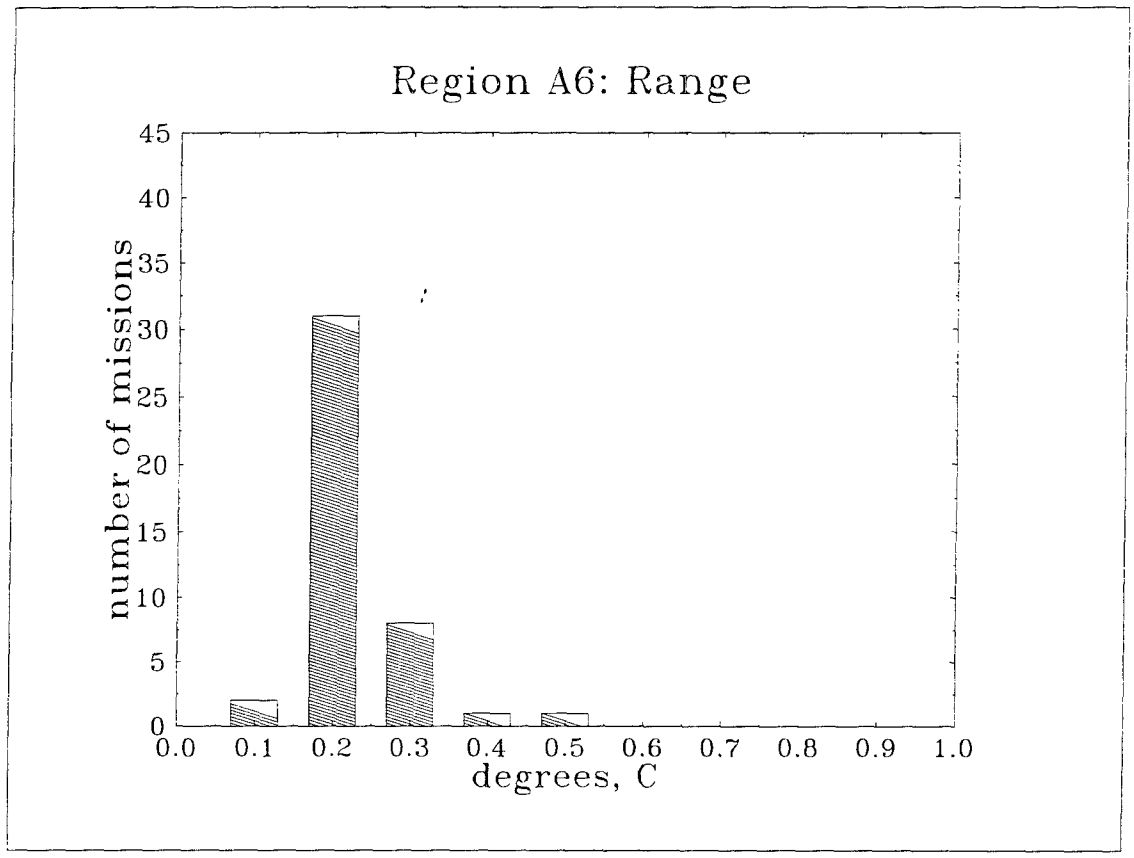

Figure A-7. Histogram of ranges of weighted, integrated apparent temperature experienced for each of the 10-s periods for the missions studied. This graph is for the mid-IR, ROI 6.

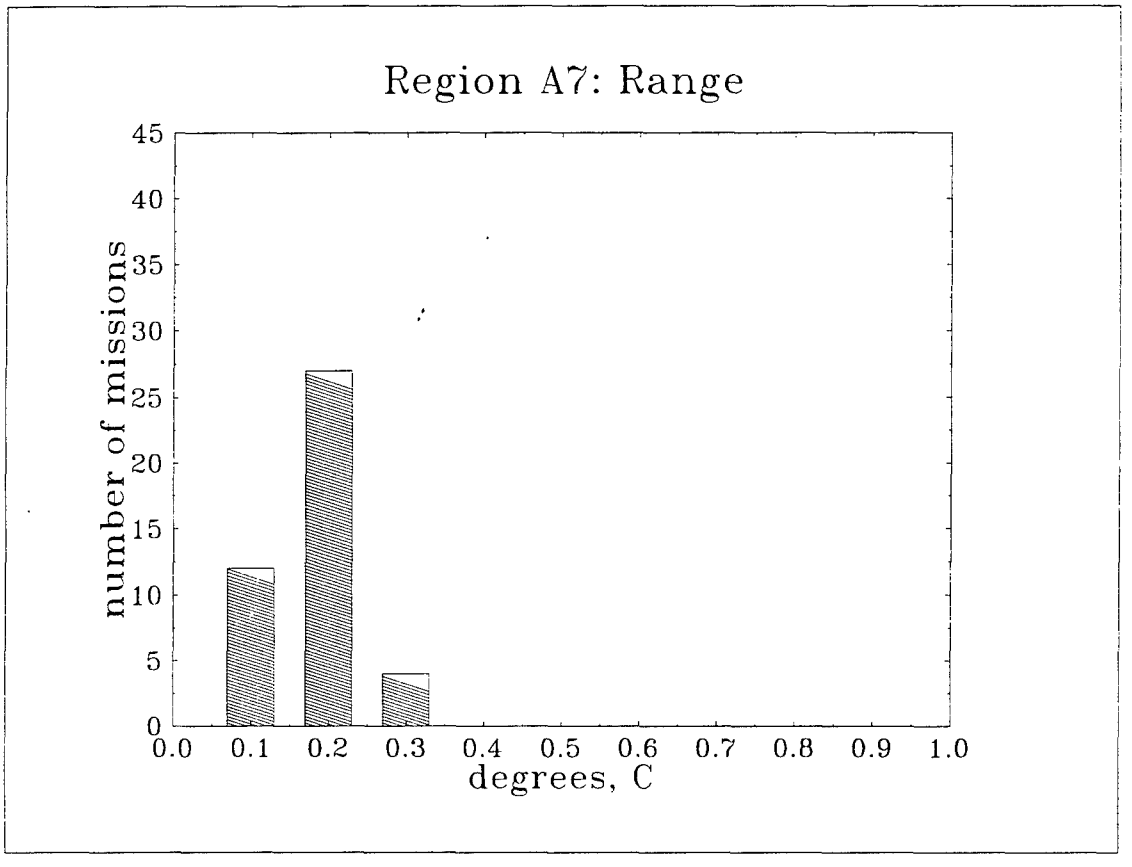

Figure A-8. Histogram of ranges of weighted, integrated apparent temperature experienced for each of the 10-s periods for the missions studied. This graph is for the mid-IR, ROI 7.

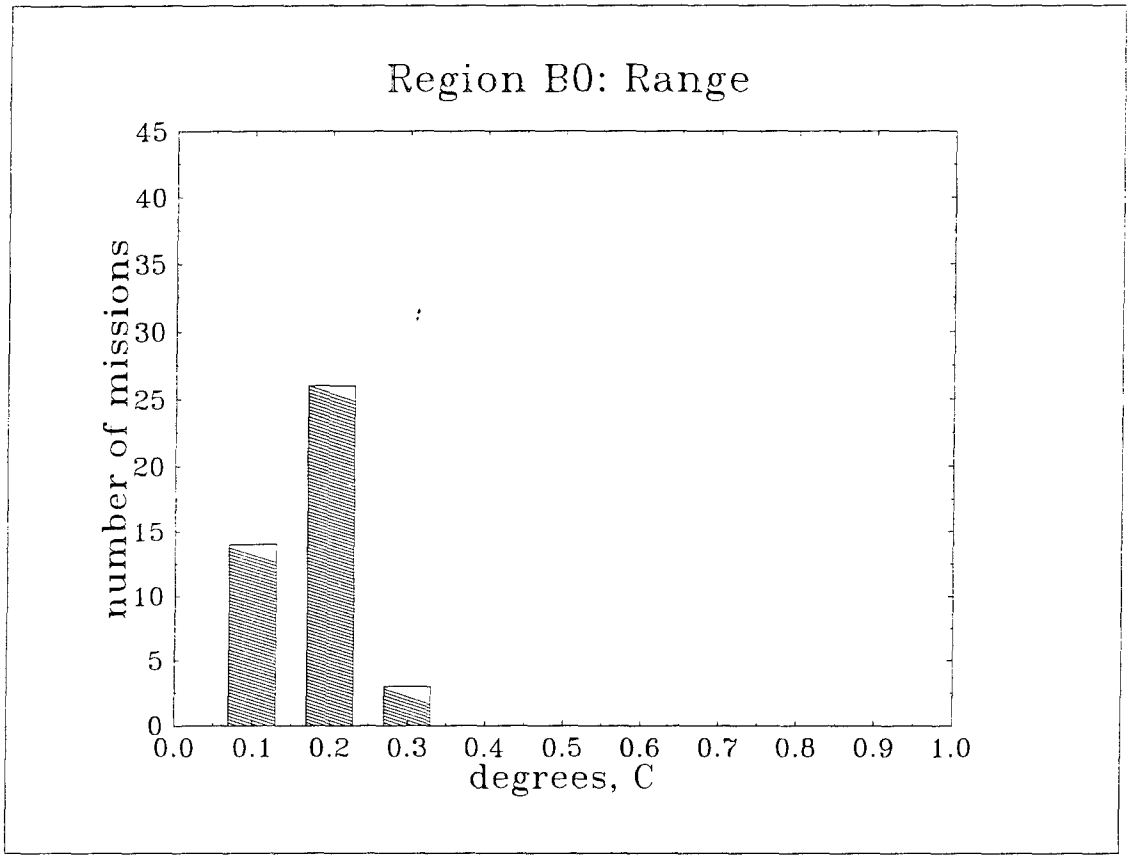

Figure A-9. Histogram of ranges of weighted, integrated apparent temperature experienced for each of the 10-s periods for the missions studied. This graph is for the far-IR, ROI 0.

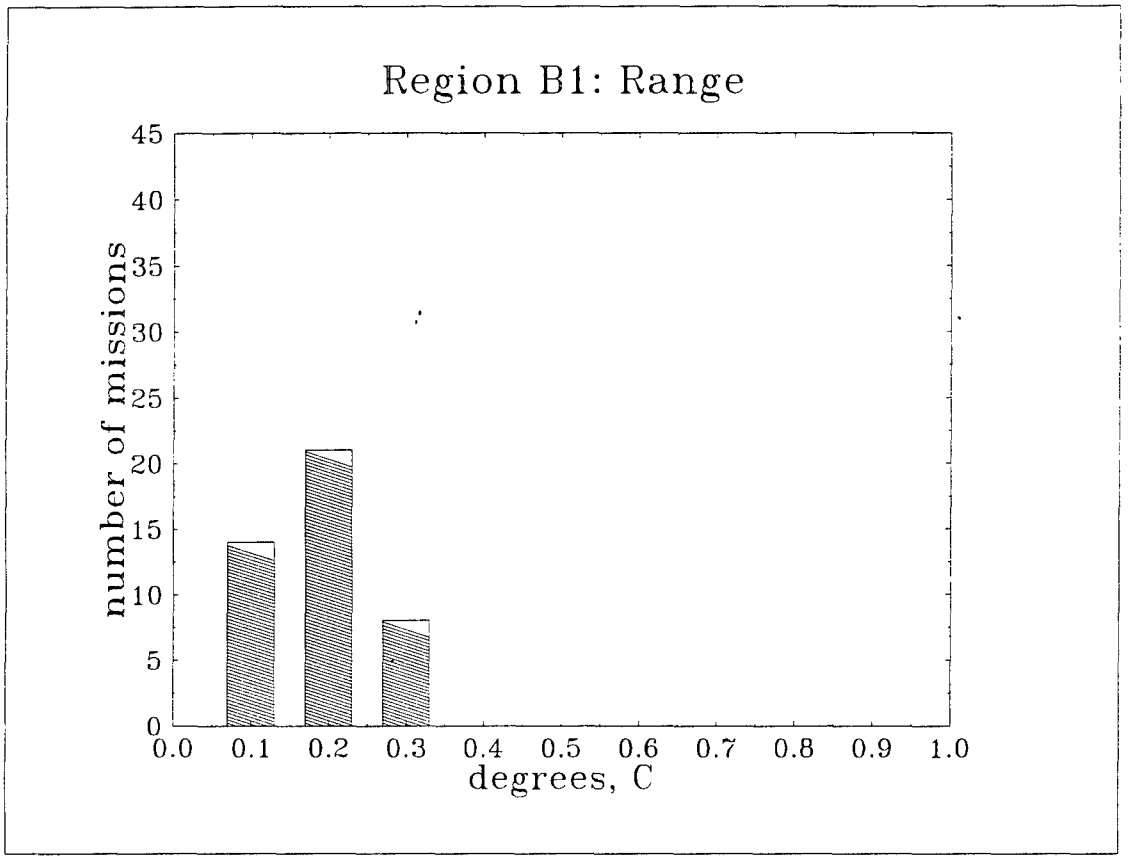

Figure A-10. Histogram of ranges of weighted, integrated apparent temperature experienced for each of the 10-s periods for the missions studied. This graph is for the far-IR, ROI 1.

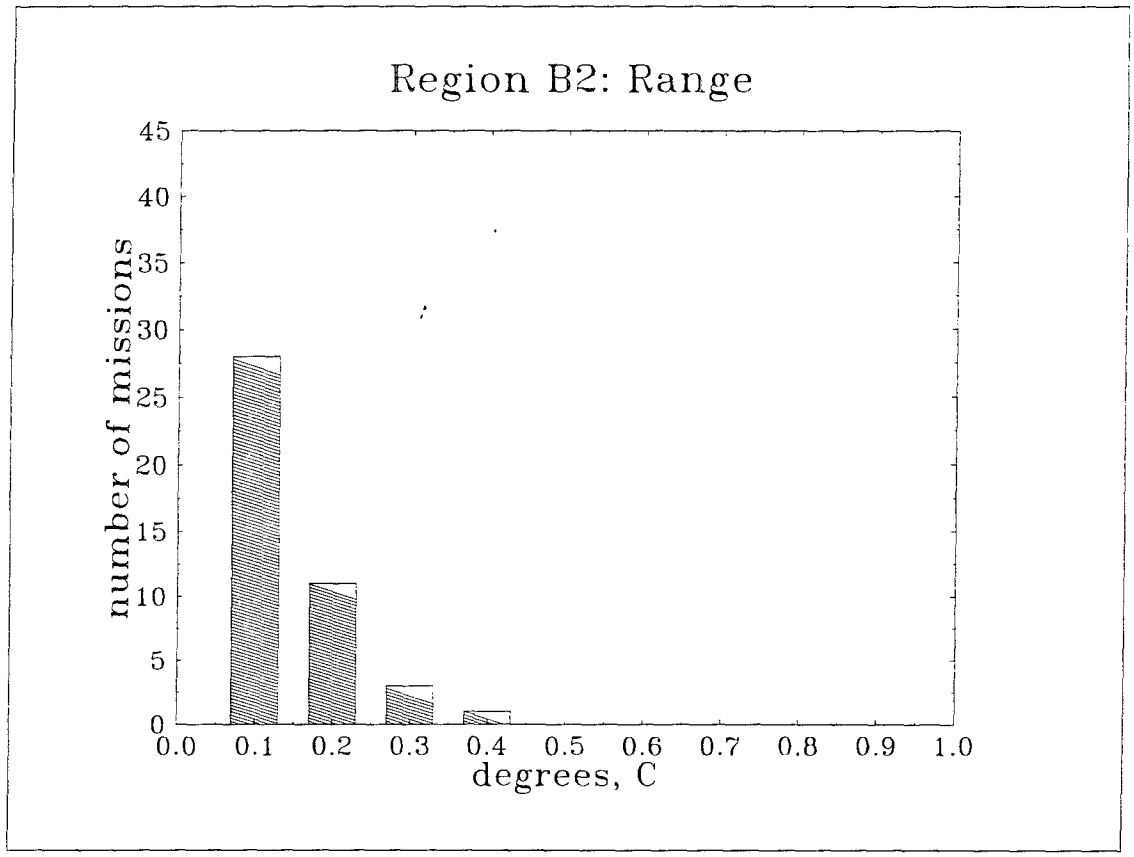

Figure A-11. Histogram of ranges of weighted, integrated apparent temperature experienced for each of the 10-s periods for the missions studied. This graph is for the far-IR, ROI 2.

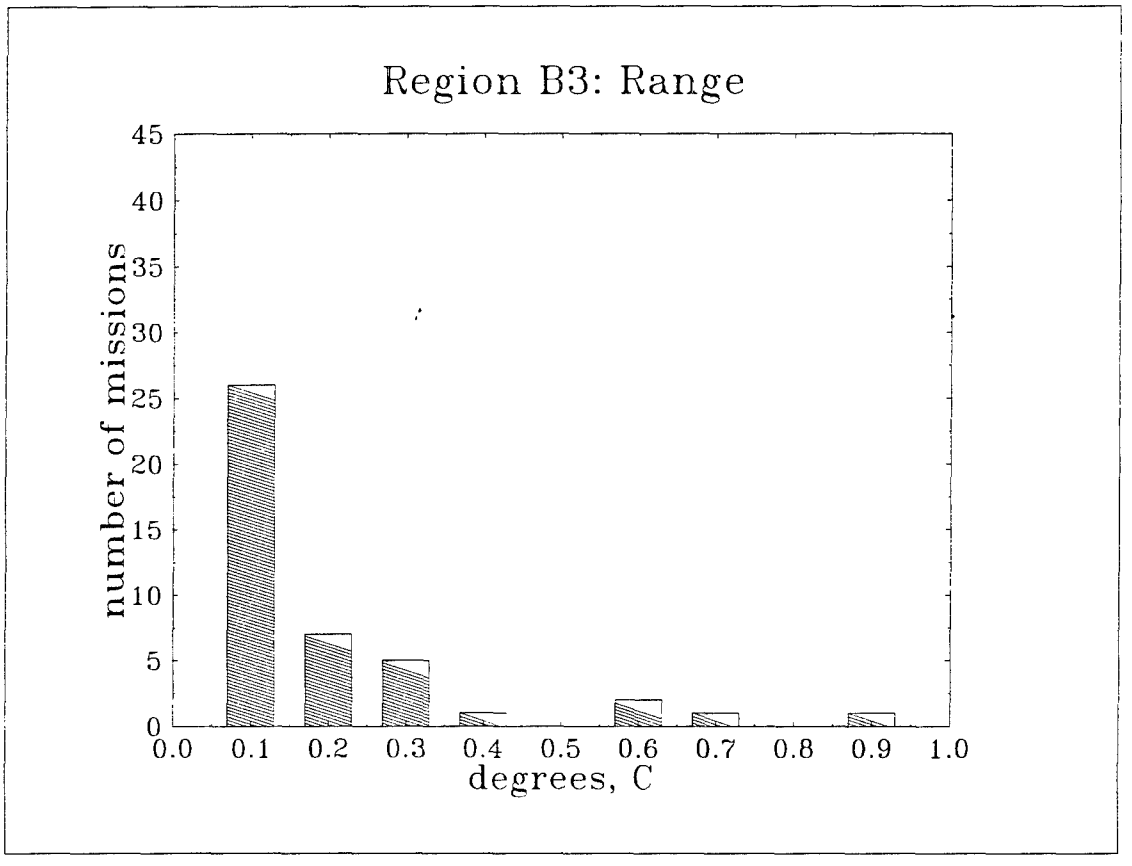

Figure A-12. Histogram of ranges of weighted, integrated apparent temperature experienced for each of the 10-s periods for the missions studied. This graph is for the far-IR, ROI 3.

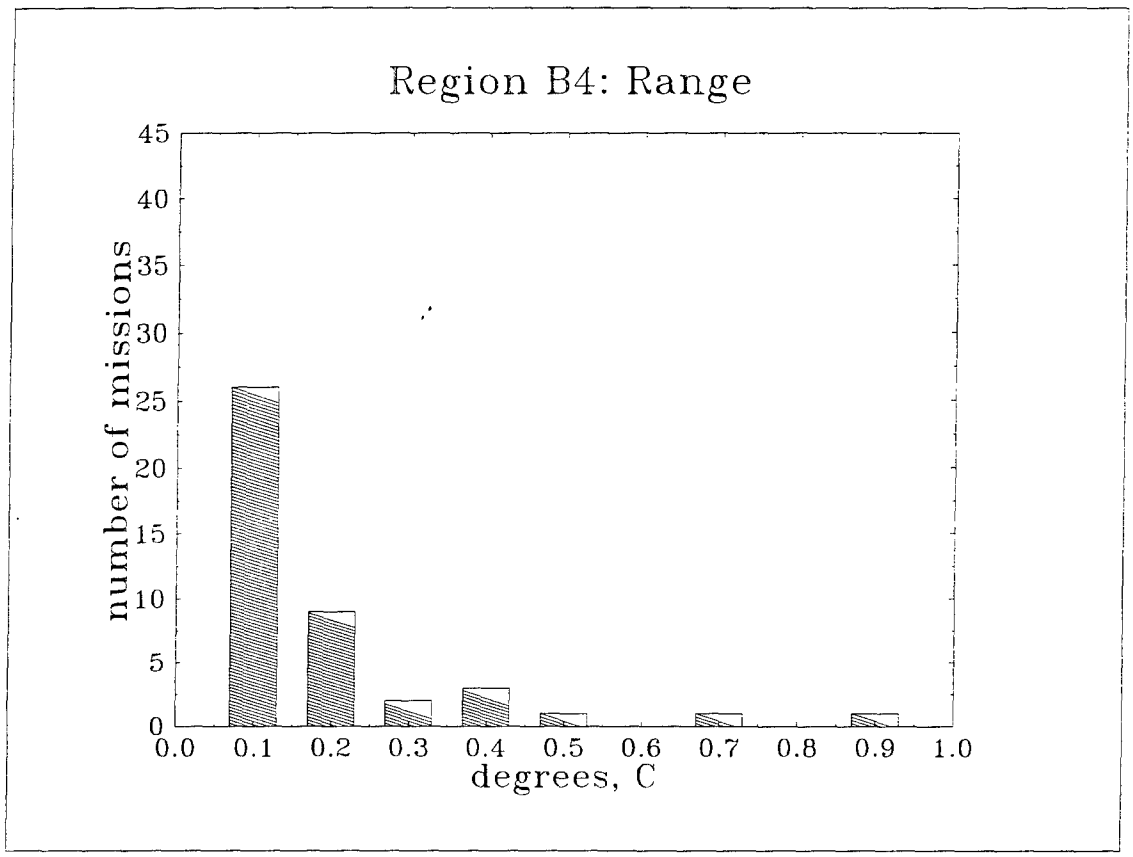

Figure A-13. Histogram of ranges of weighted, integrated apparent temperature experienced for each of the 10-s periods for the missions studied. This graph is for the far-IR, ROI 4.

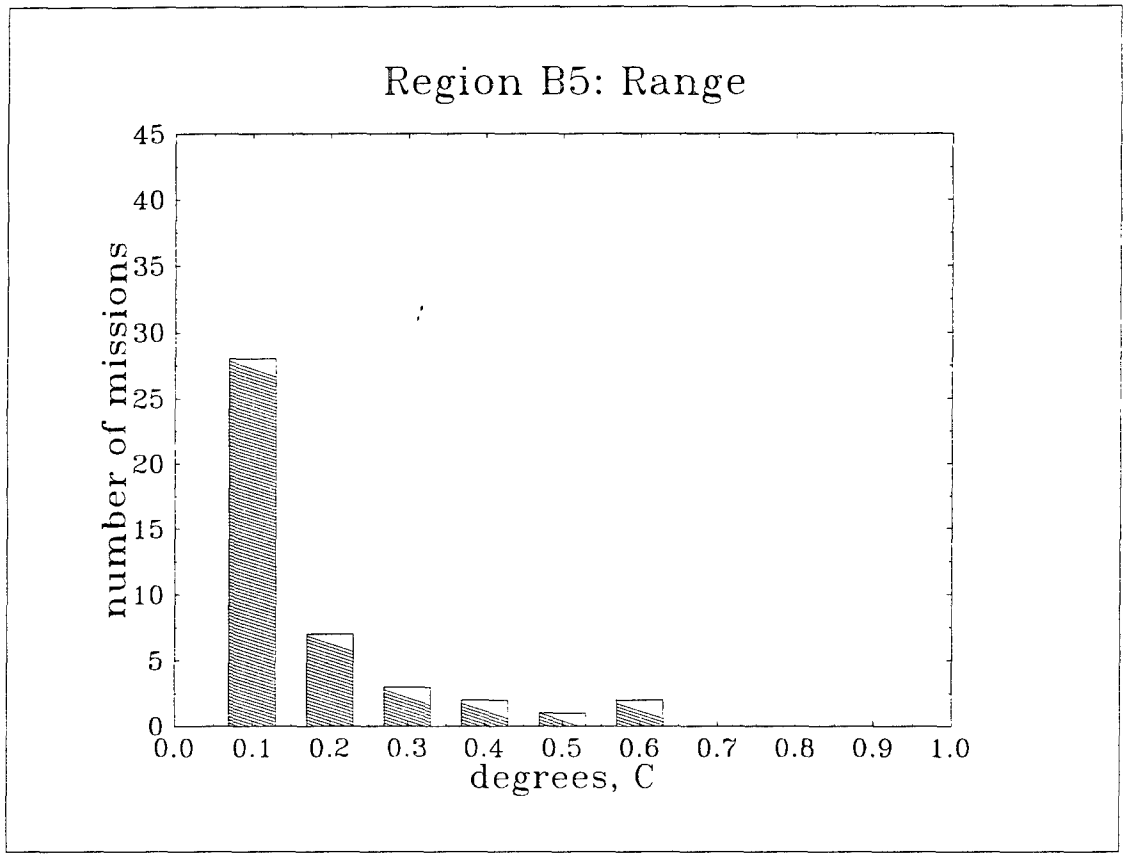

Figure A-14. Histogram of ranges of weighted, integrated apparent temperature experienced for each of the 10-s periods for the missions studied. This graph is for the far-IR, ROI 5.

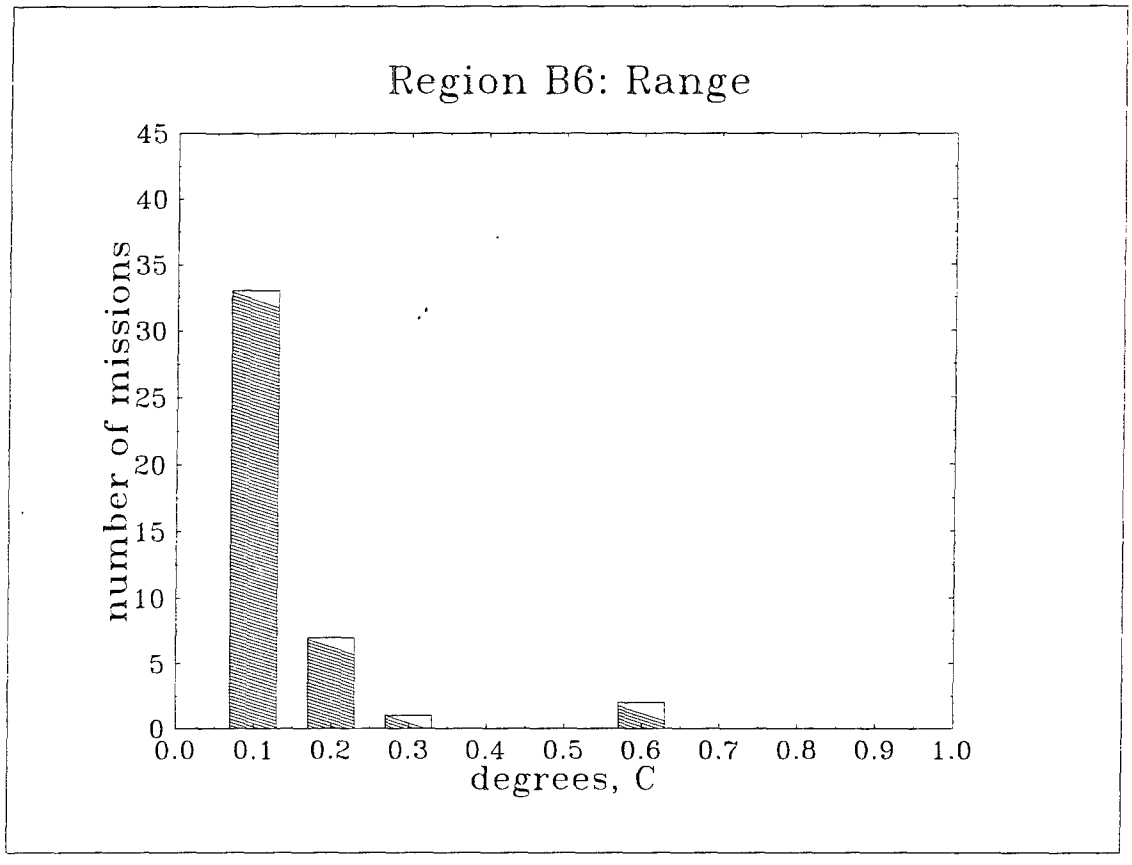

Figure A-15. Histogram of ranges of weighted, integrated apparent temperature experienced for each of the 10-s periods for the missions studied. This graph is for the far-IR, ROI 6.

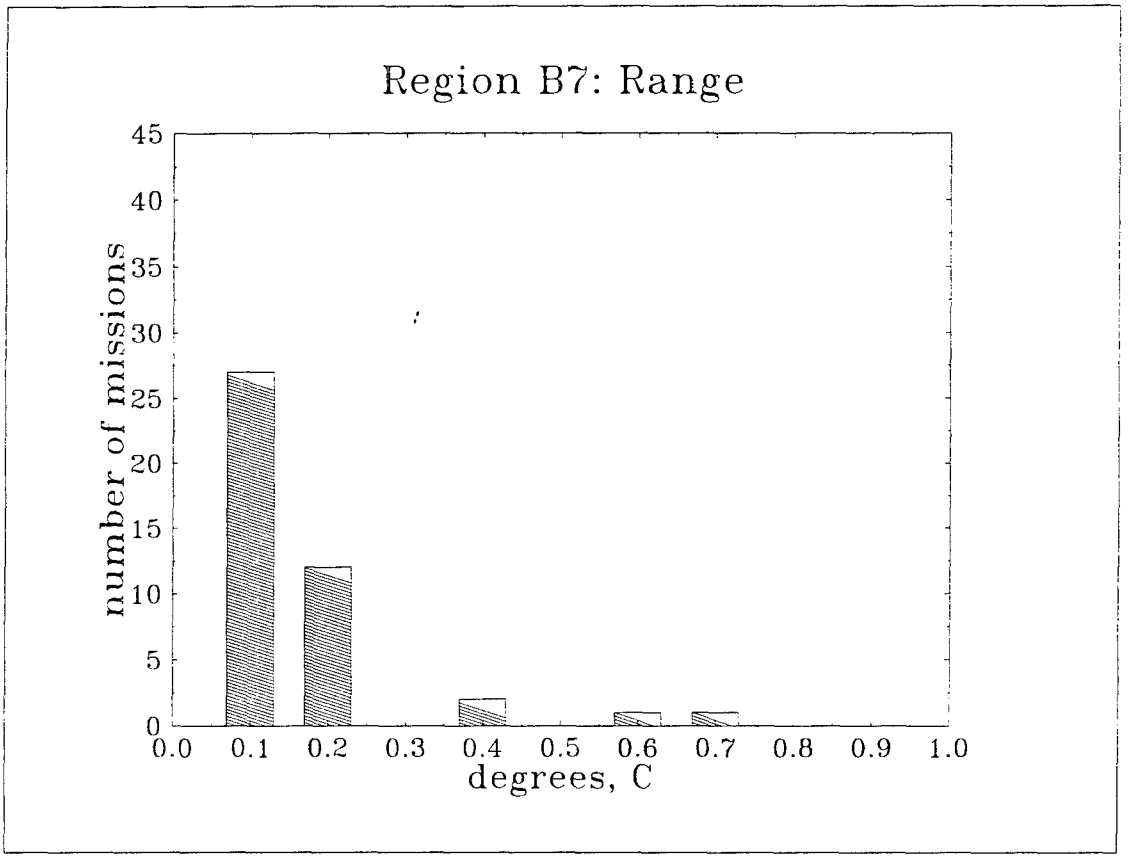

Figure A-16. Histogram of ranges of weighted, integrated apparent temperature experienced for each of the 10-s periods for the missions studied. This graph is for the far-IR, ROI 7.

Appendix B

Plots of the 10-s Average Apparent Temperature, at 5-min Intervals, for the First Hour of Missions 17, 40, and 48.

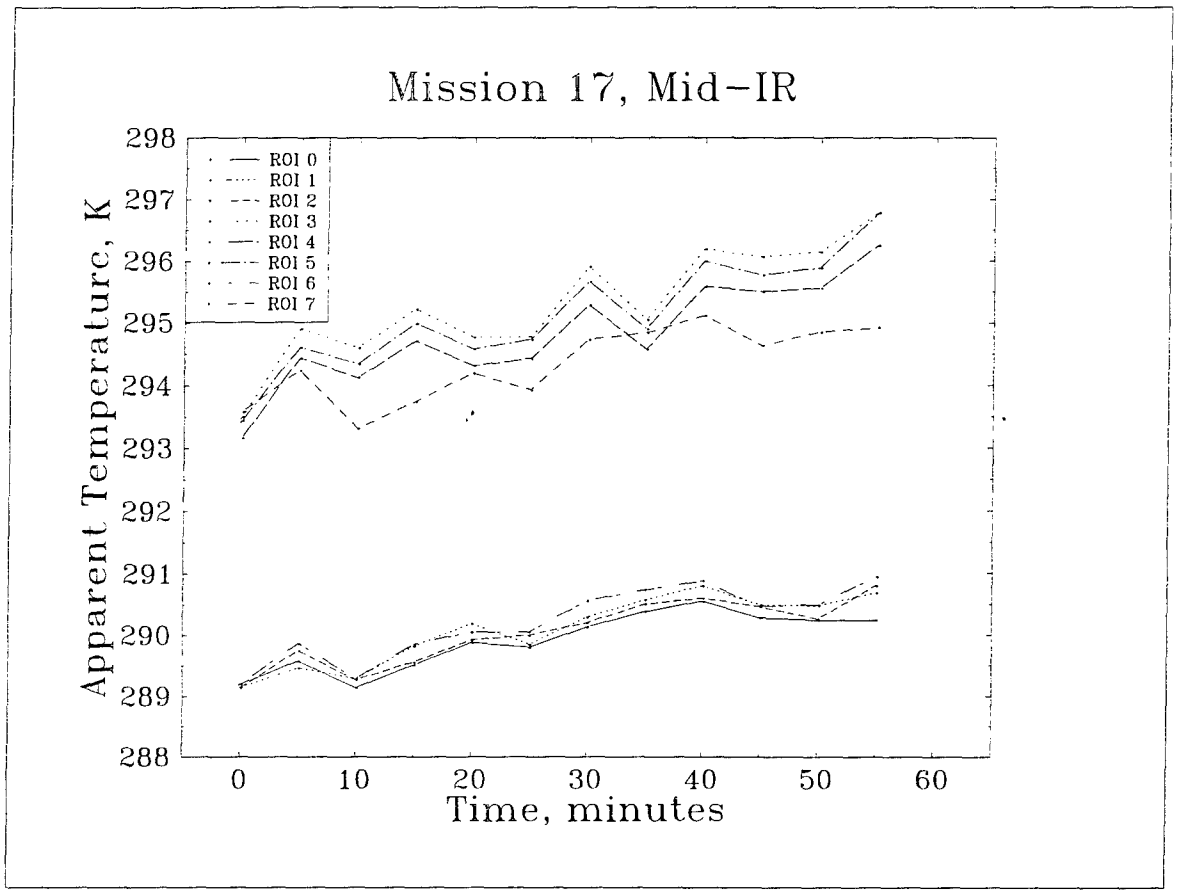

Figure B-1. For Mission 17, mid-IR, the 10-s average apparent temperature for the seven ROIs at 5-min. intervals. The reader is referred to table 2 for more detailed information; it is the intent, instead, that these figures be used to get a sense of the trends during the observation period.

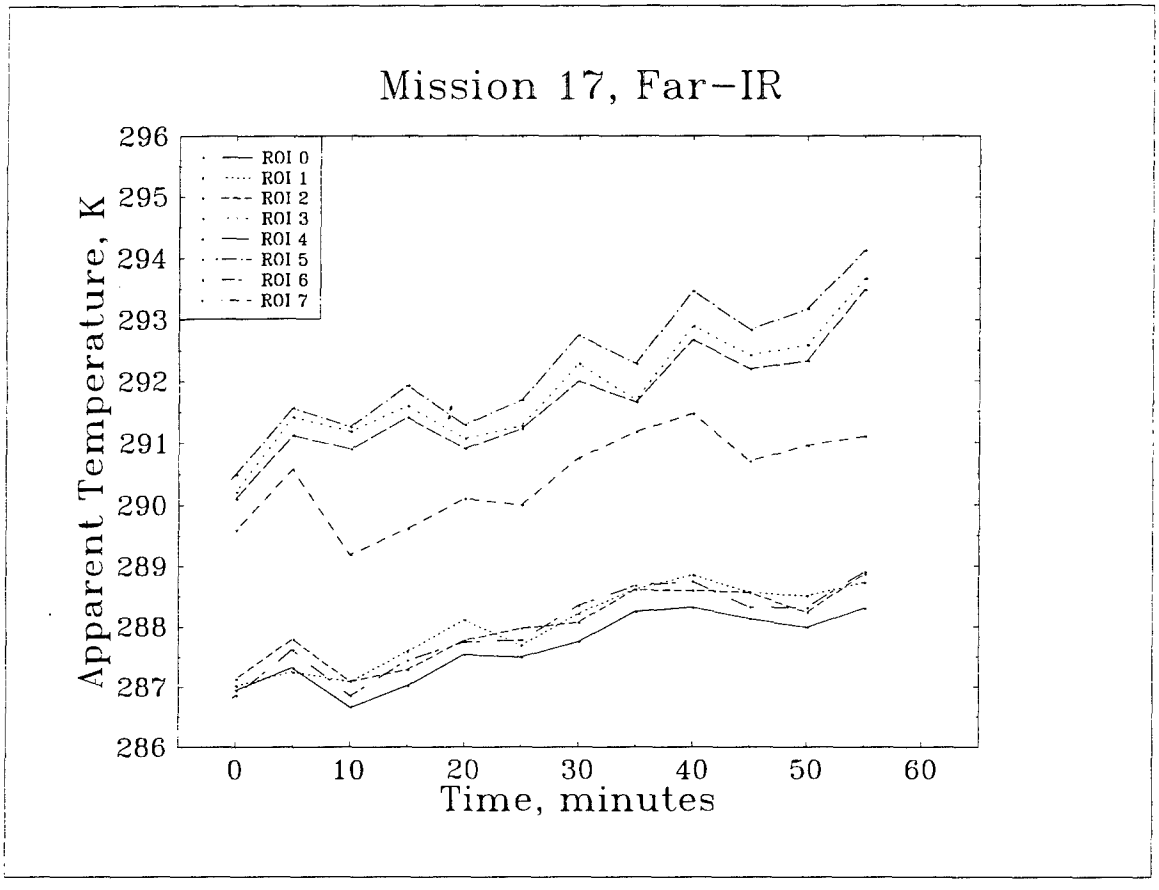

Figure B-2. For Mission 17, far-IR, the 10-s average apparent temperature for the seven ROIs at 5-min. intervals. The reader is referred to table 2 for more detailed information; it is the intent, instead, that these figures be used to get a sense of the trends during the observation period.

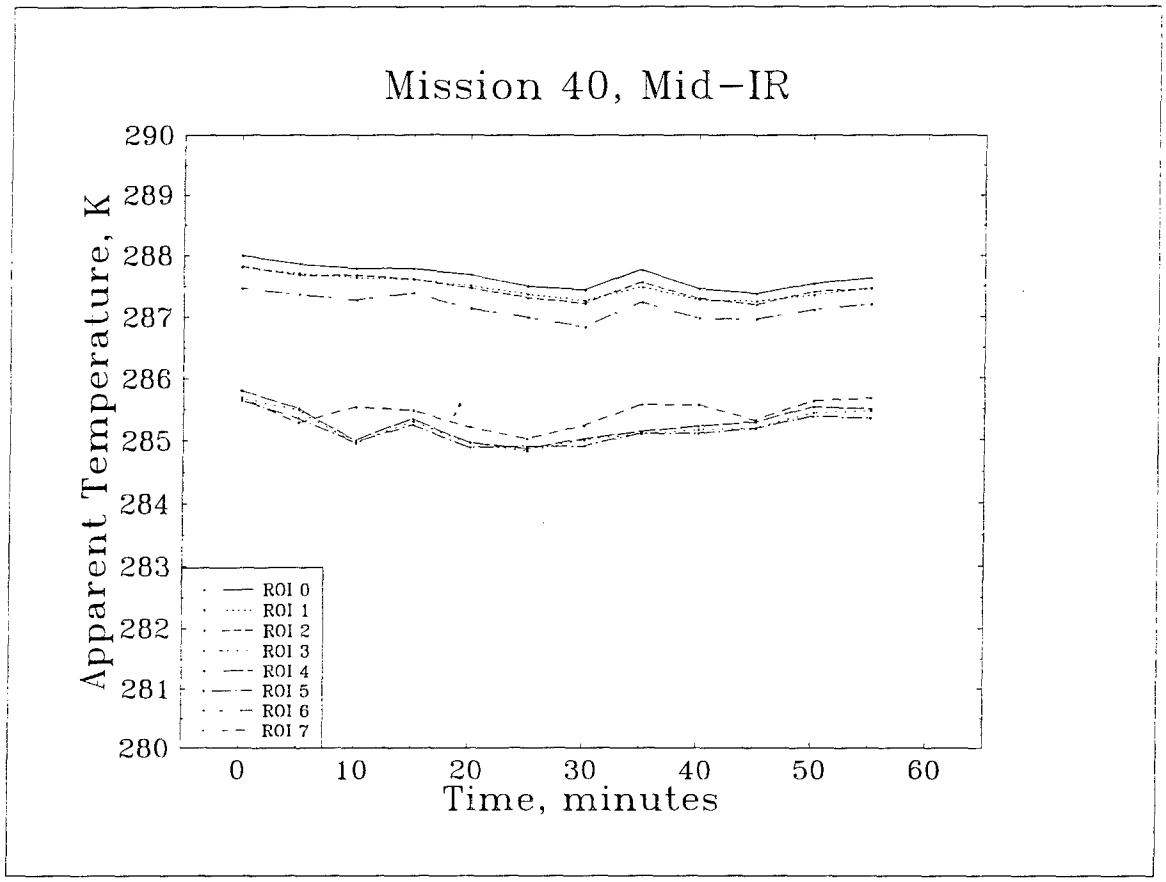

Figure B-3. For Mission 40, mid-IR, the 10-s average apparent temperature for the eight ROIs at 5-min. intervals. The reader is referred to table 2 for more detailed information; it is the intent, instead that these figures be used to get a sense of the trends during the observation period.

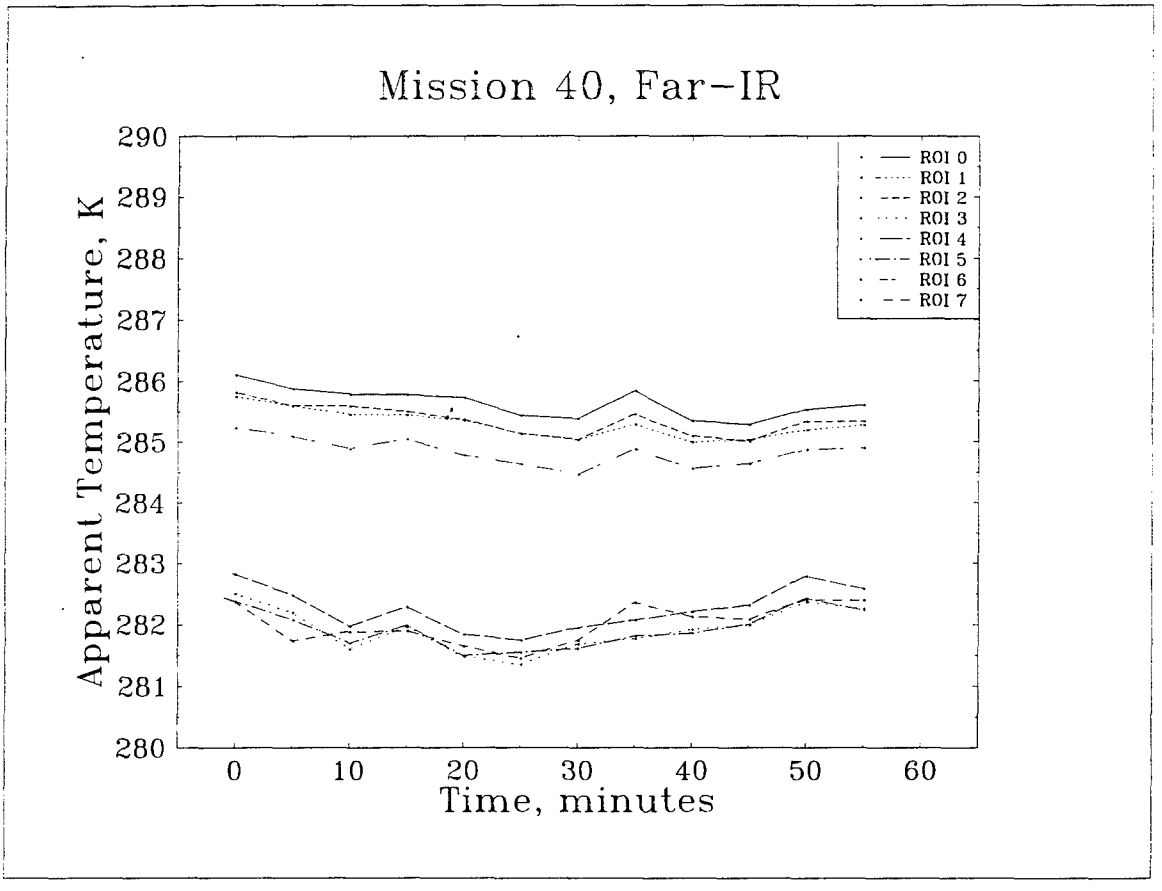

Figure B-4. For Mission 40, far-IR, the 10-s average apparent temperature for the eight ROIs at 5-min. intervals. The reader is referred to table 2 for more detailed information; it is the intent, instead that these figures be used to get a sense of the trends during the observation period.

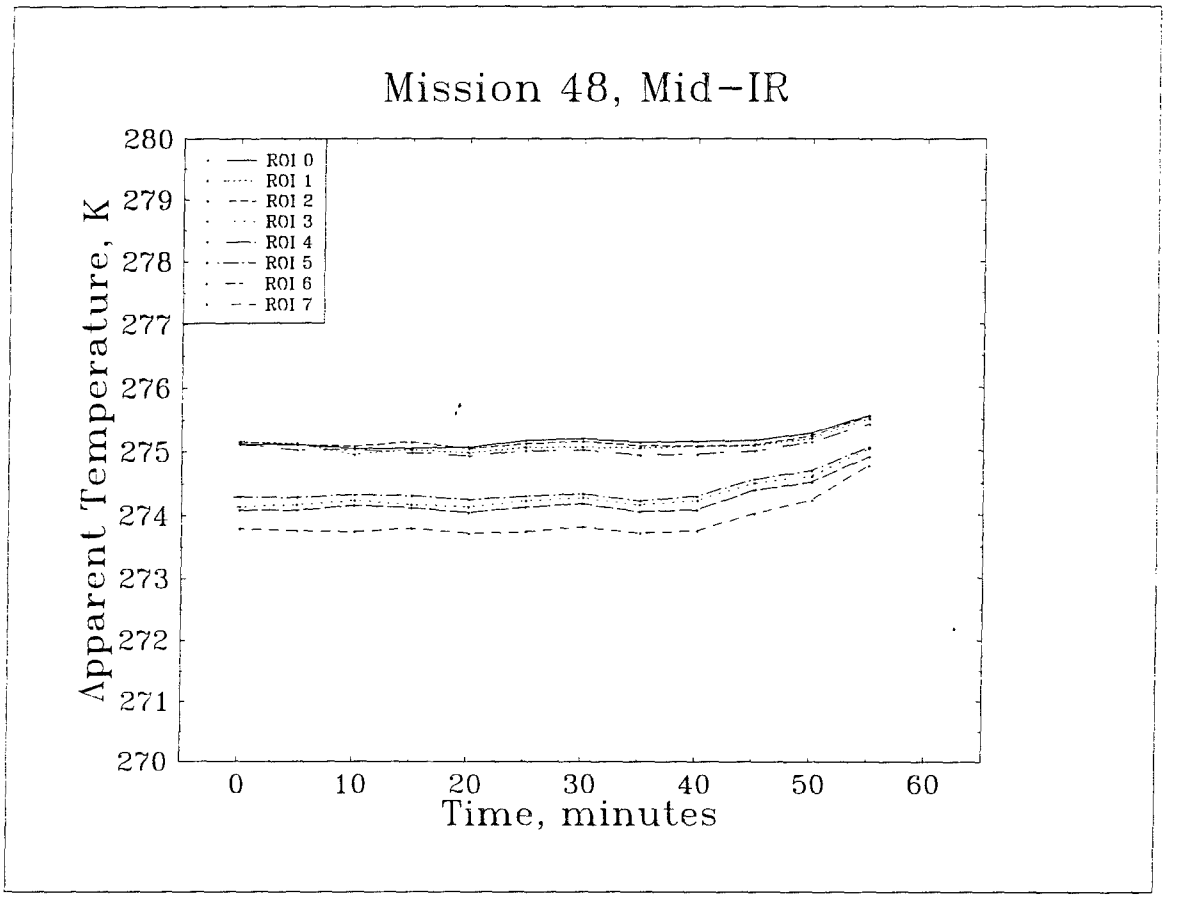

Figure B-5. For Mission 48, mid-IR, the 10-s average apparent temperature for the eight ROIs at 5-min. intervals. The reader is referred to table 2 for more detailed information; it is the intent, instead that these figures be used to get a sense of the trends during the observation period.

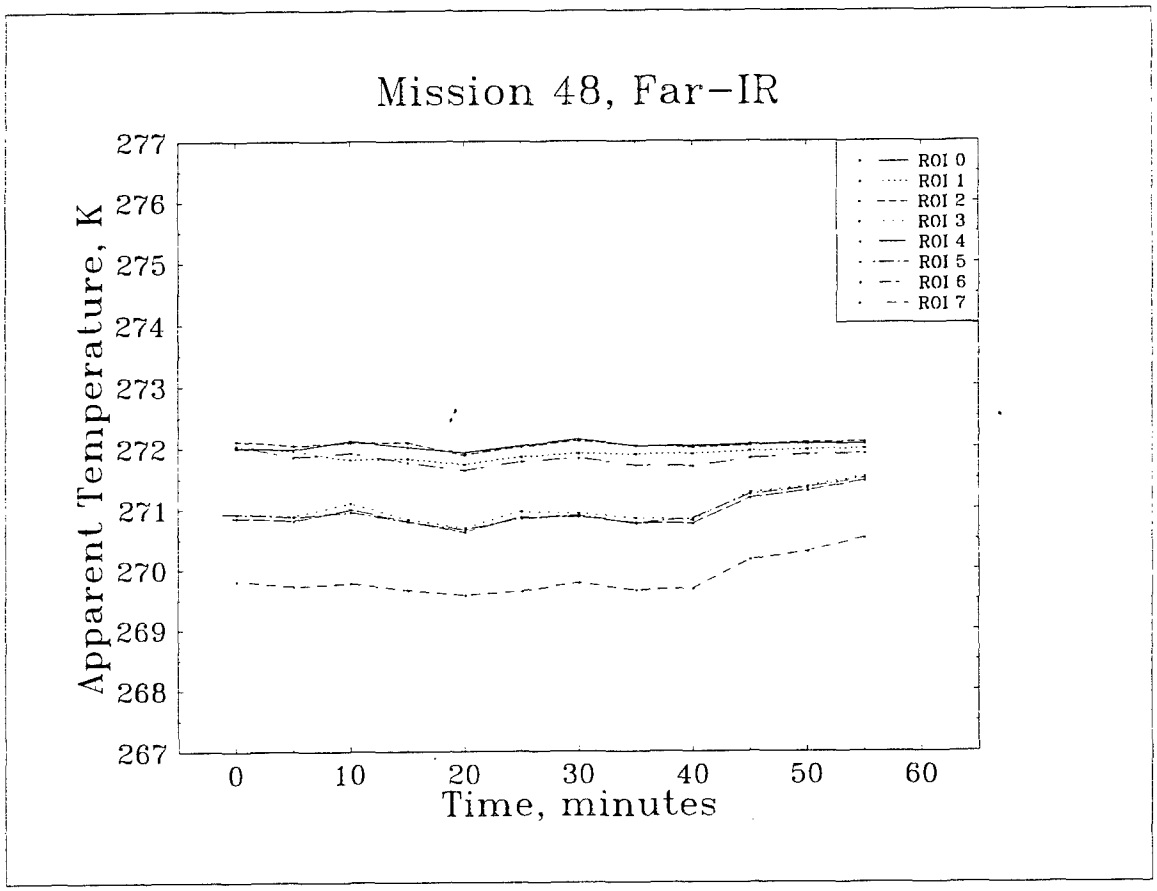

Figure B-6. For Mission 48, far-IR, the 10-s average apparent temperature for the eight ROIs at 5-min. intervals. The reader is referred to table 2 for more detailed information; it is the intent, instead that these figures be used to get a sense of the trends during the observation period.

Appendix C

Plots of the Range in Average Apparent Temperature During the 10-s Period, at 5-min Intervals, for the First Hour of Missions 17, 40 , and 48.

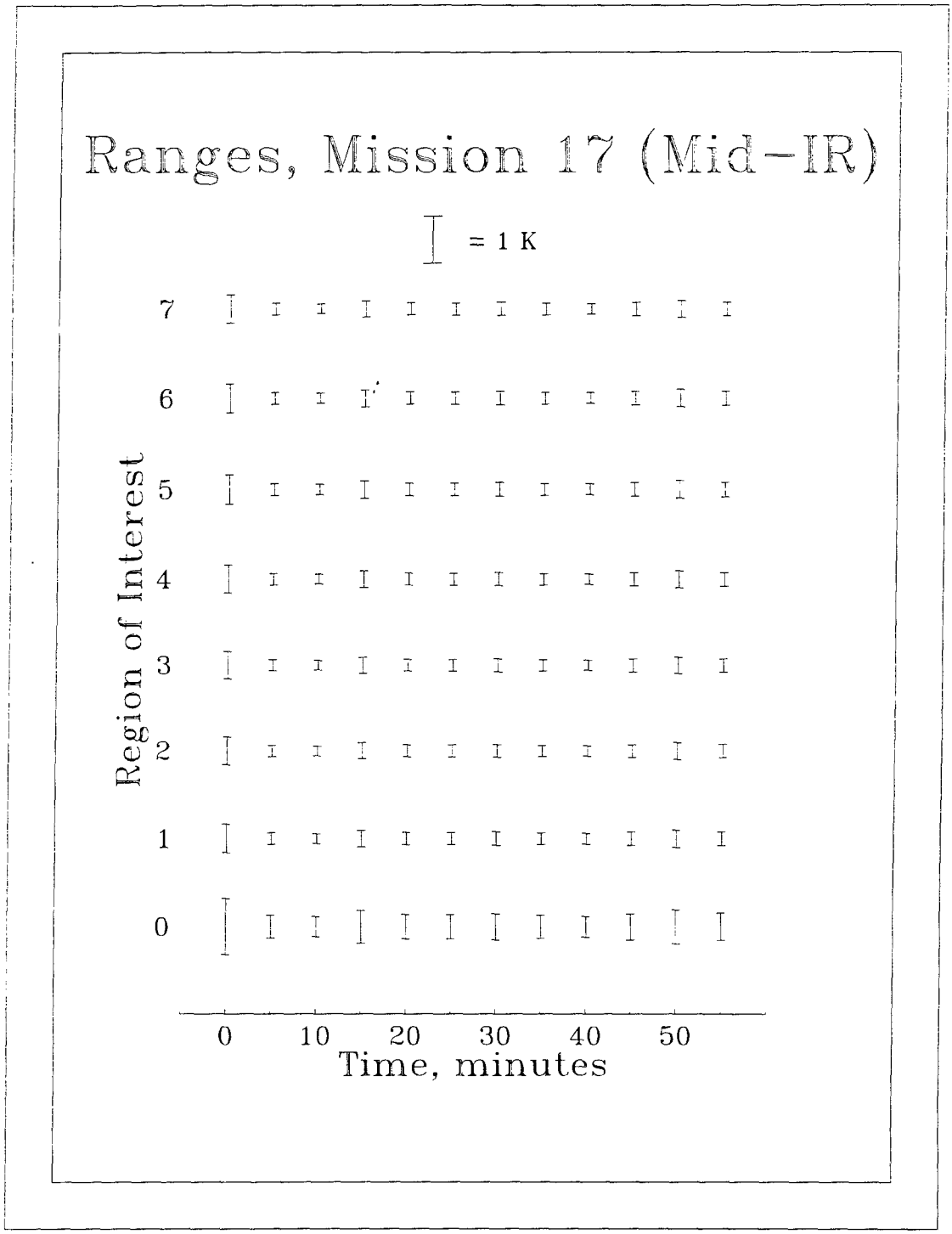

Figure C-1. Plot of the range in apparent temperature for each of the 10-s periods and ROIs. This plot is for mission 17, mid-IR.

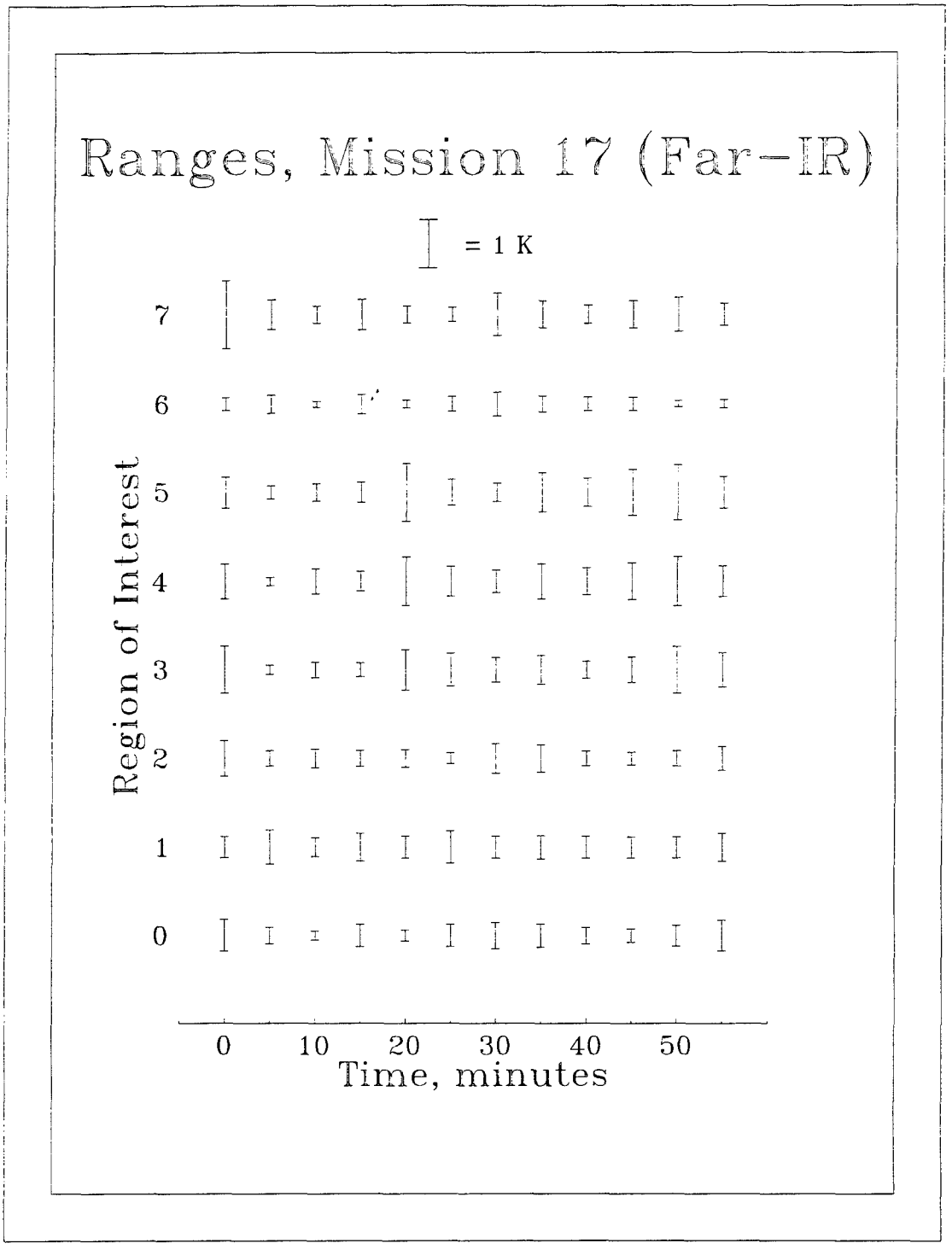

Figure C-2. Plot of the range in apparent temperature for each of the 10-s periods and ROIs. This plot is for mission 17, far-IR.

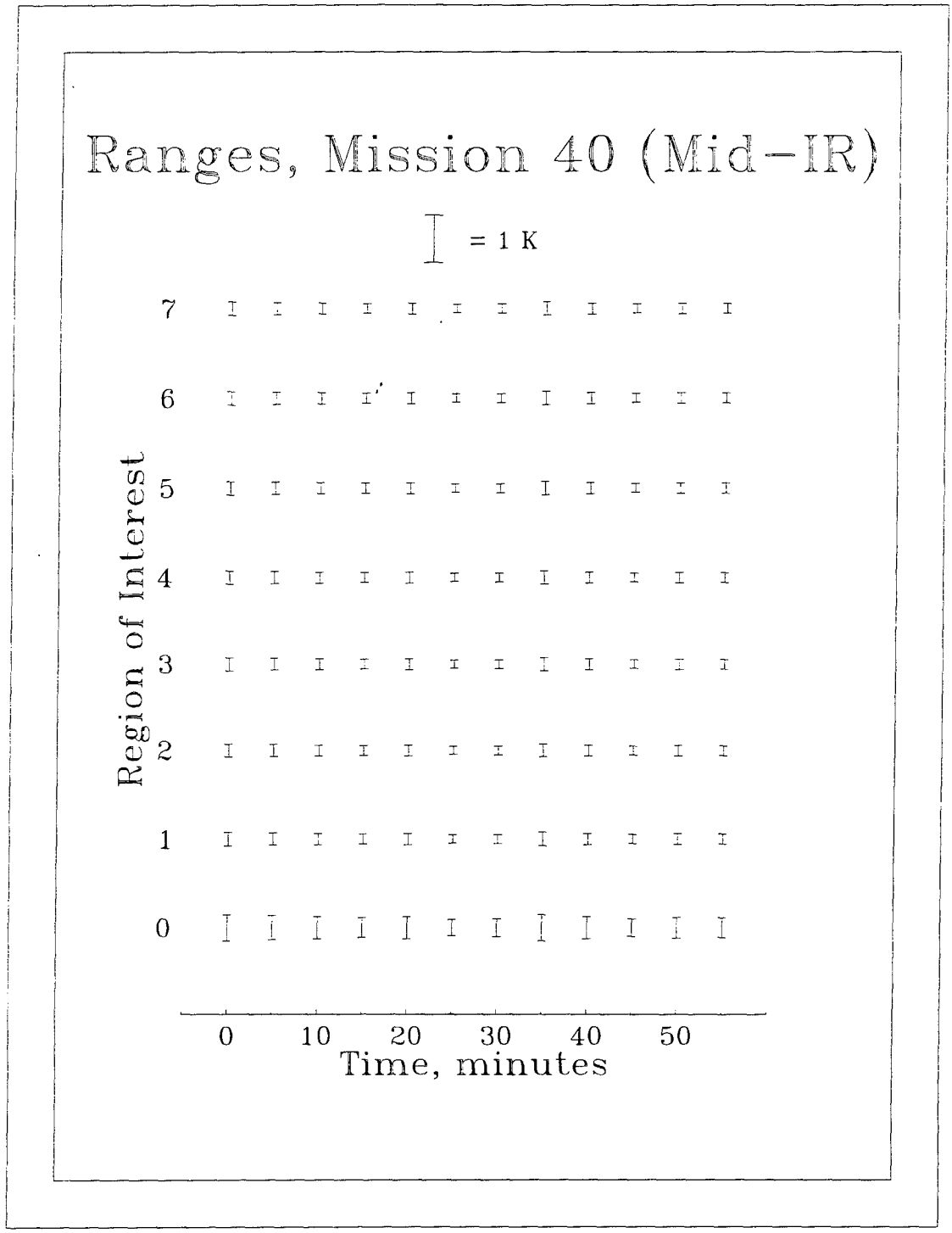

Figure C-3. Plot of the range in apparent temperature for each of the 10-s periods and ROIs. This plot is for mission 40, mid-IR.

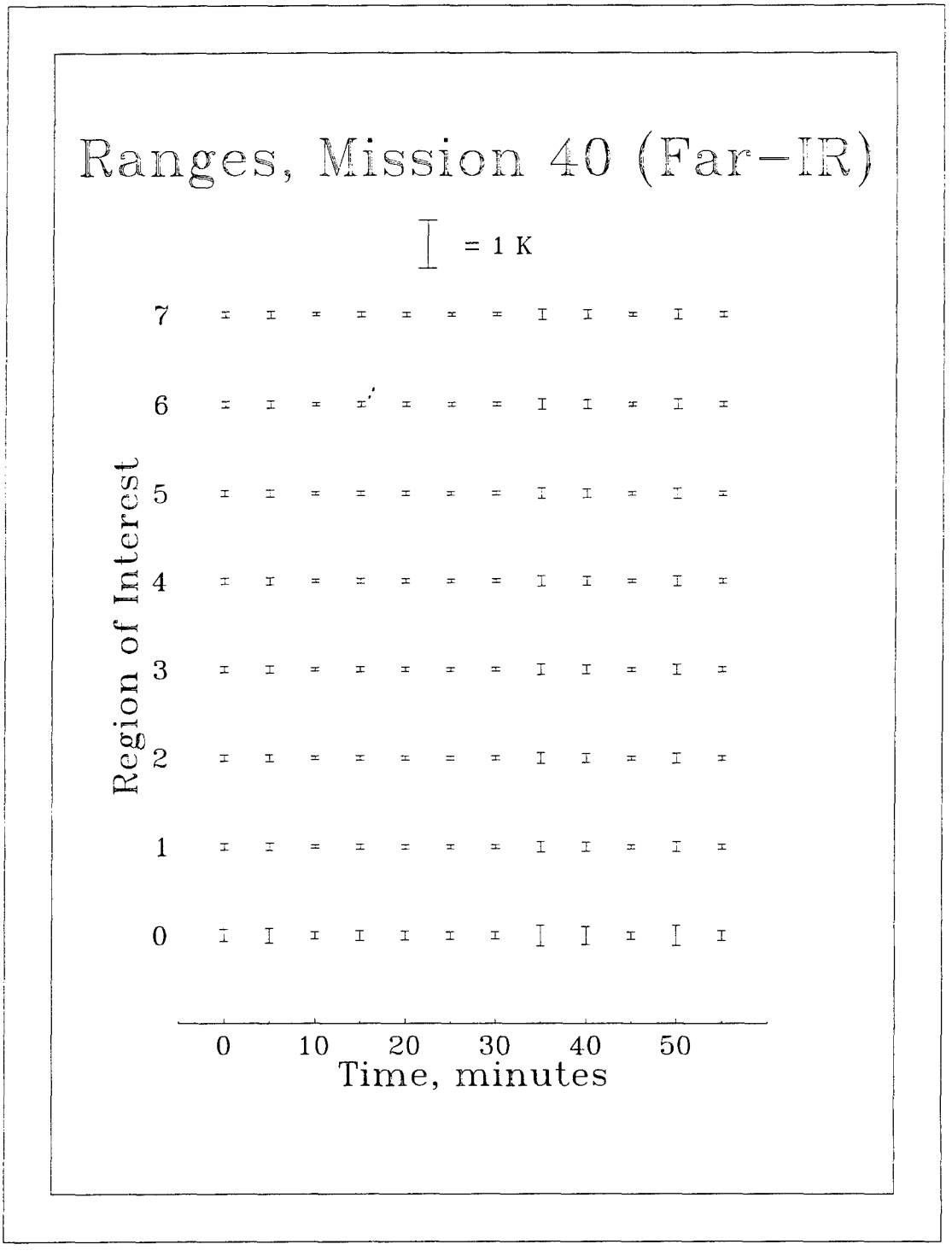

Figure C-4. Plot of the range in apparent temperature for each of the 10-s periods and ROIs. This plot is for mission 40, far-IR.

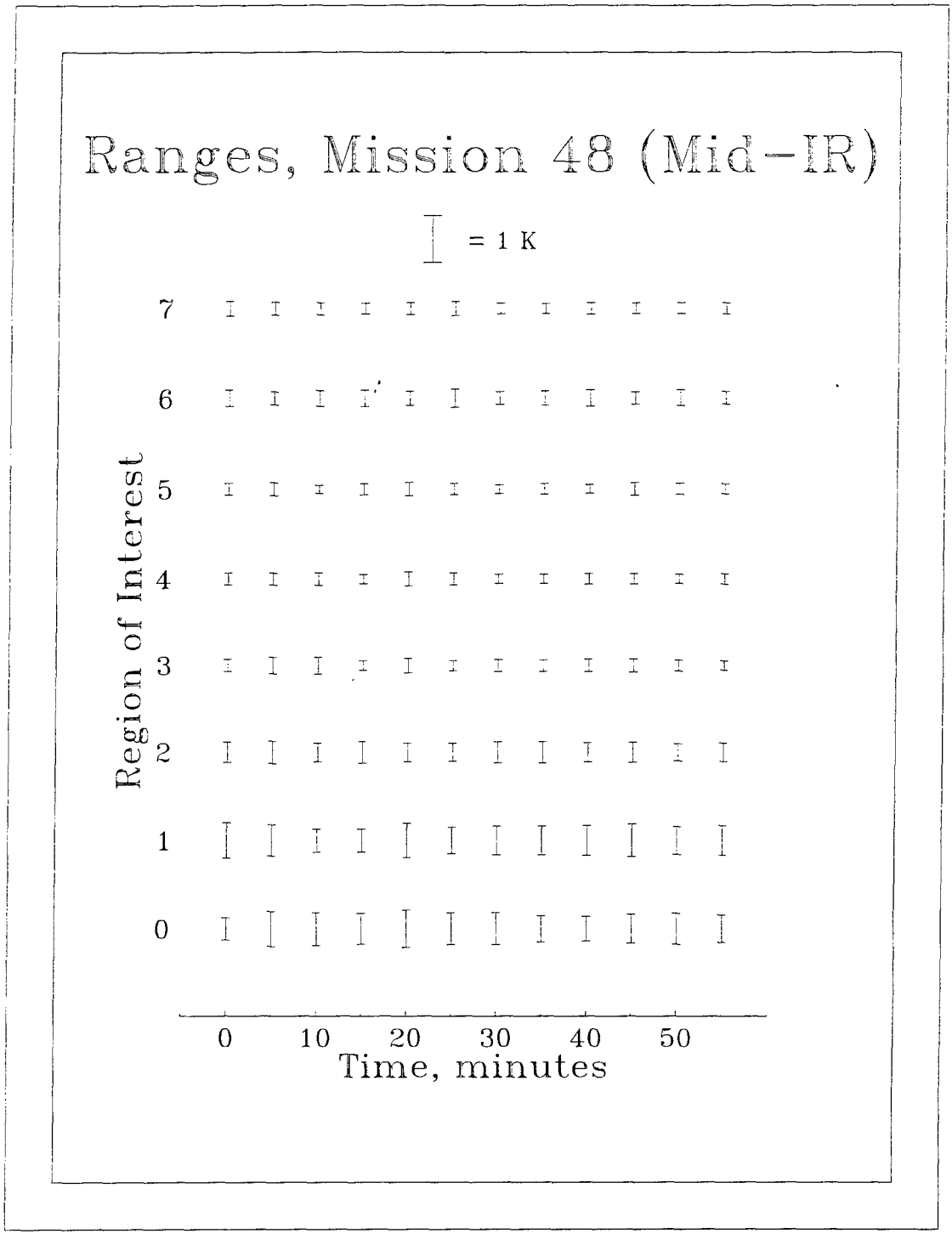

Figure C-5. Plot of the range in apparent temperature for each of the 10-s periods and ROIs. This plot is for mission 48, mid-IR.

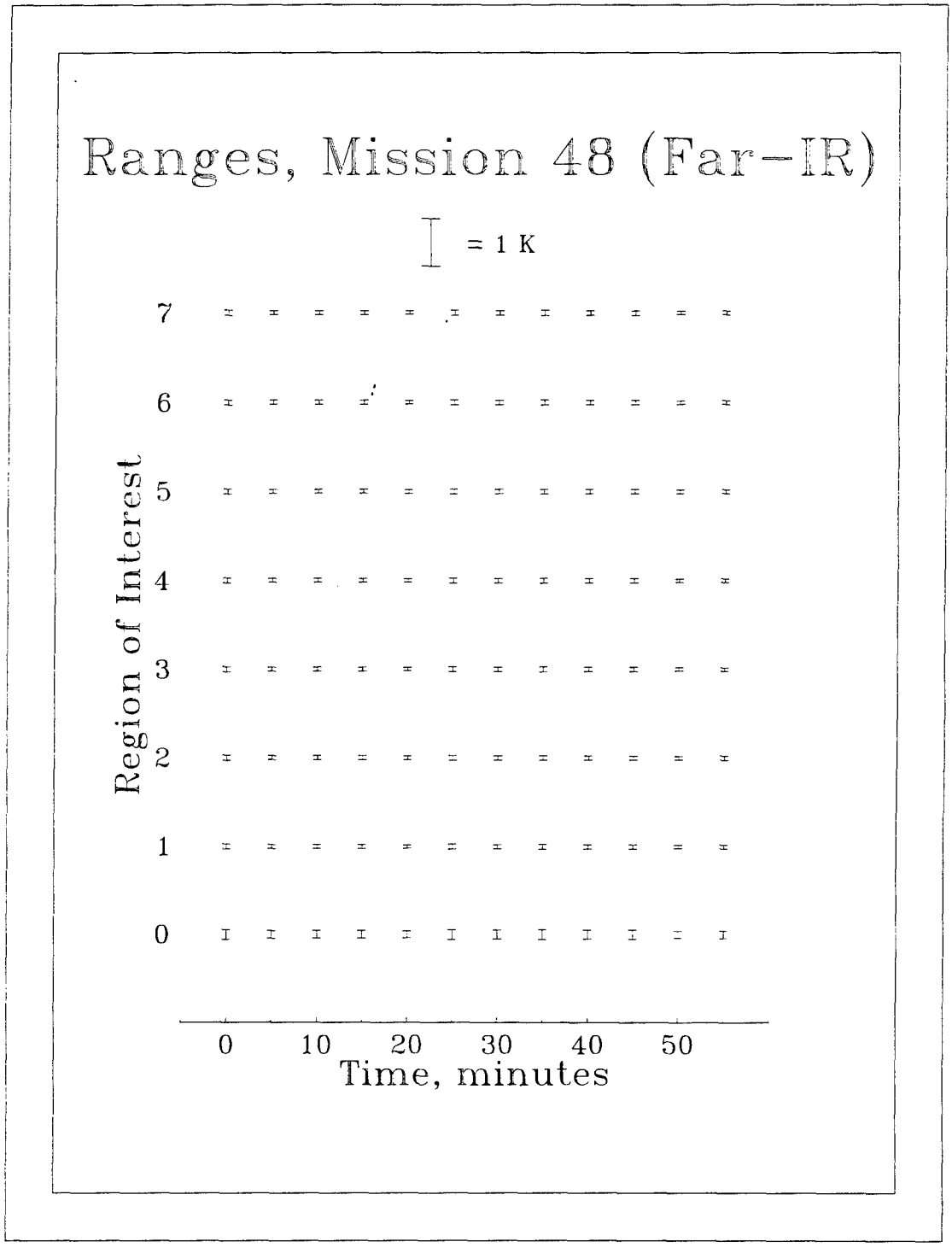

Figure C-6. Plot of the range in apparent temperature for each of the 10-s periods and ROIs. This plot is for mission 48, far-IR.

Appendix D

Plots of Several Meteorological Variables, as Measured During the First Hour of the Three Missions Under Study.

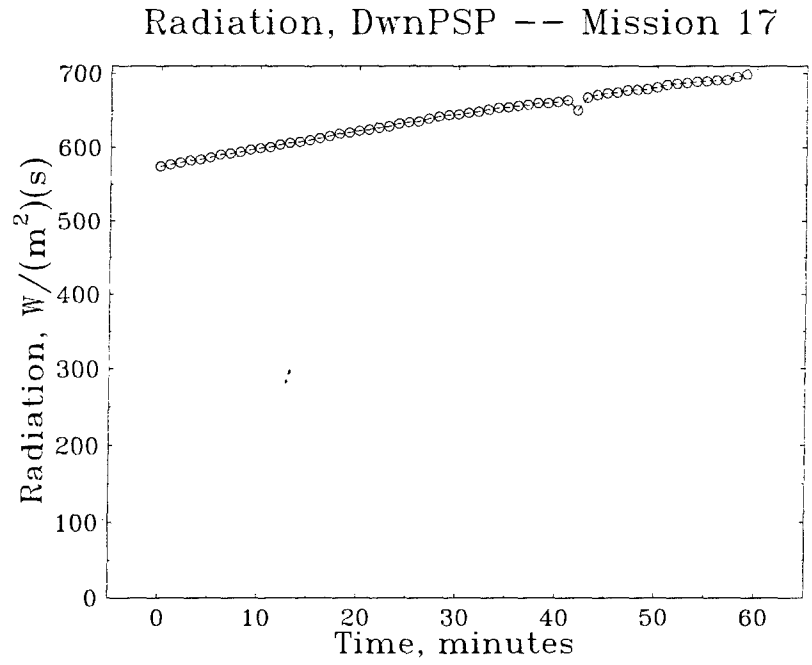

Figure D-1. Downwelling PSP radiation during the first hour of mission 17.

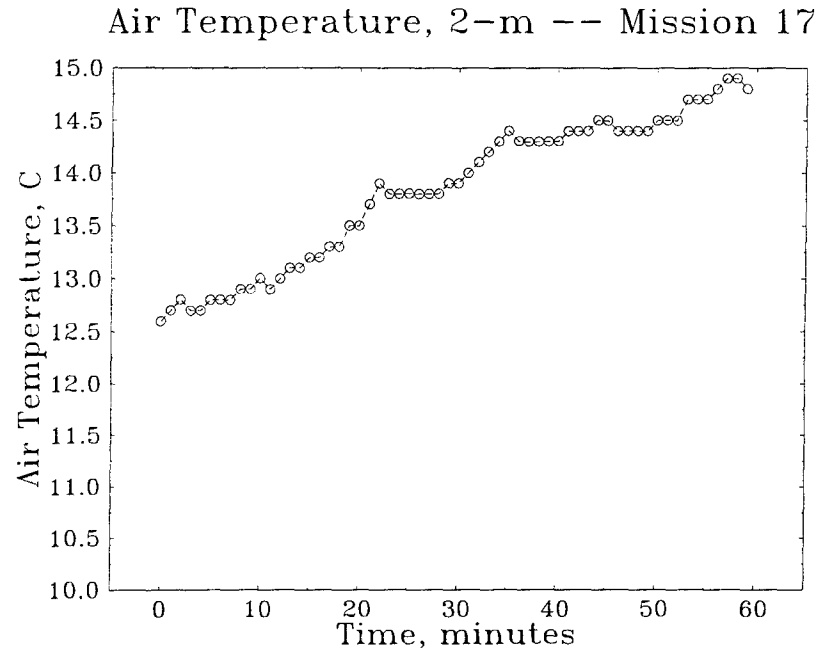

Figure D-2. Air temperature at 2m (AGL) during the first hour of mission 17.

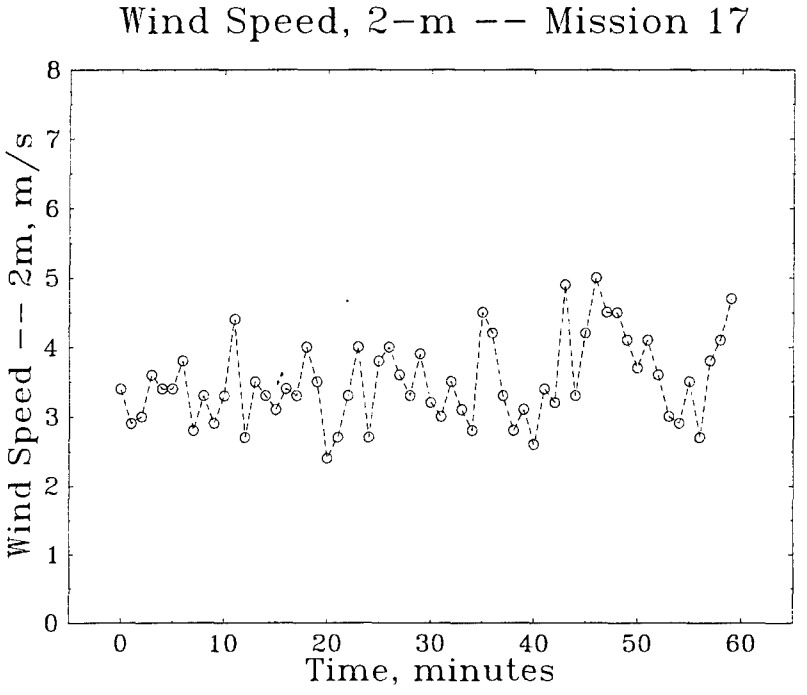

Figure D-3. Wind speed at 2m (AGL) during the first hour of mission 17.

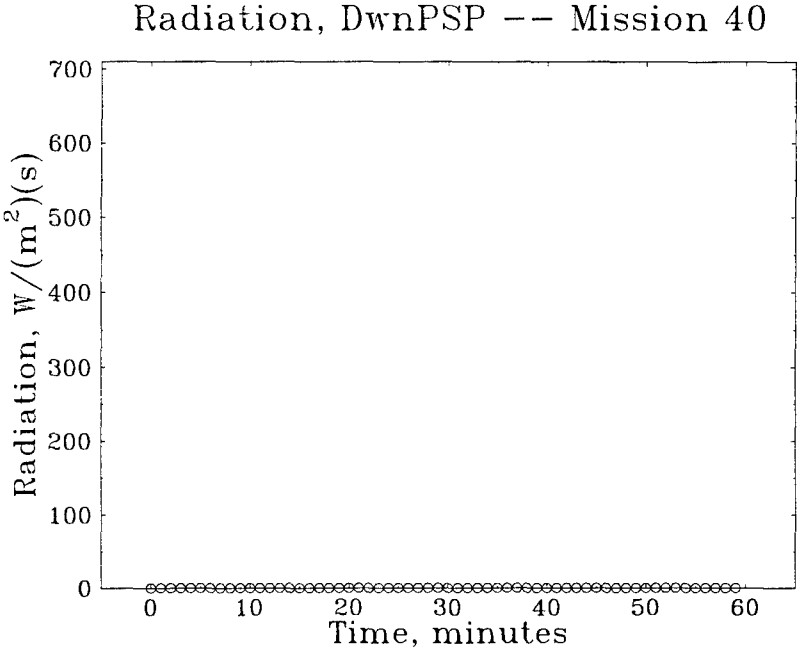

Figure D-4. Downwelling PSP radiation during the first hour of mission 40.

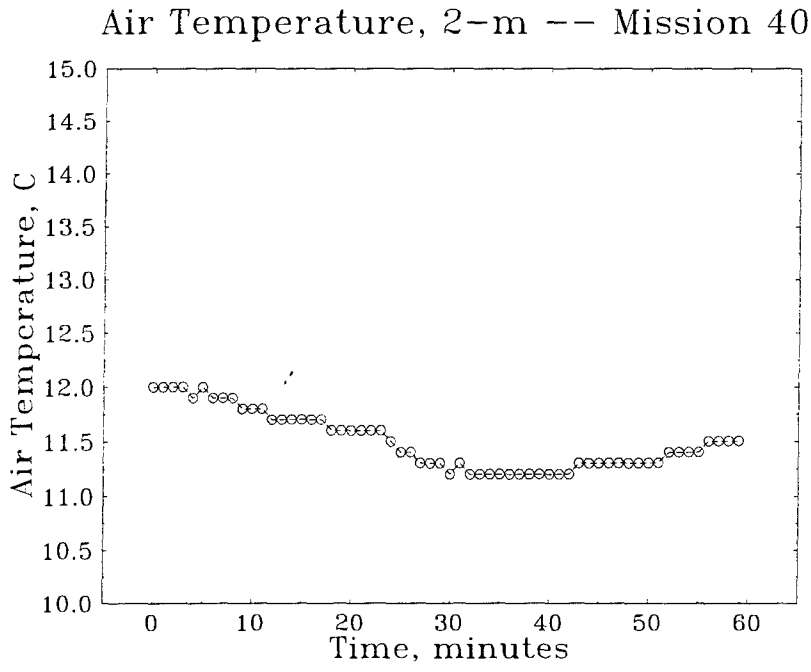

Figure D-5. Air temperature at 2m (AGL) during the first hour of mission 40.

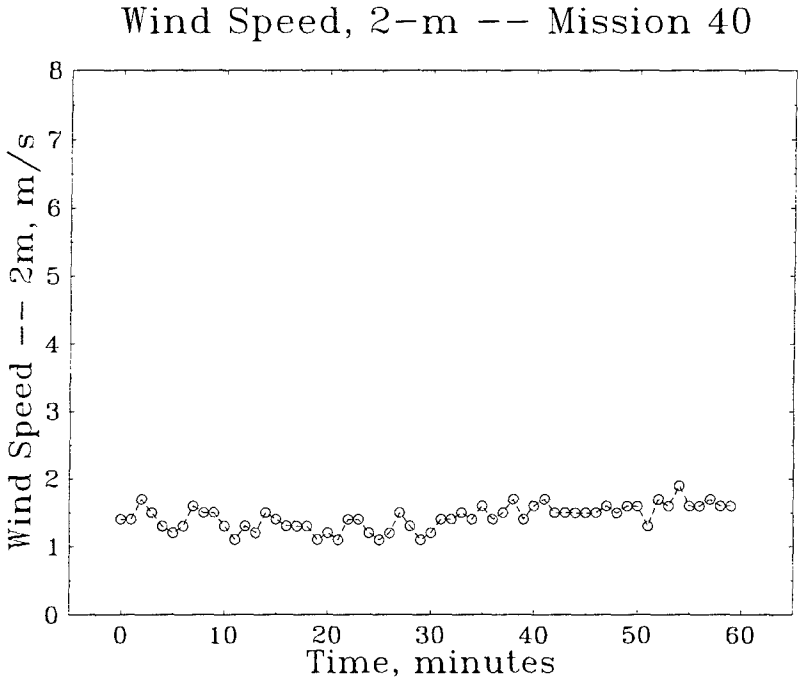

Figure D-6. Wind speed at 2m (AGL) during the first hour of mission 40.

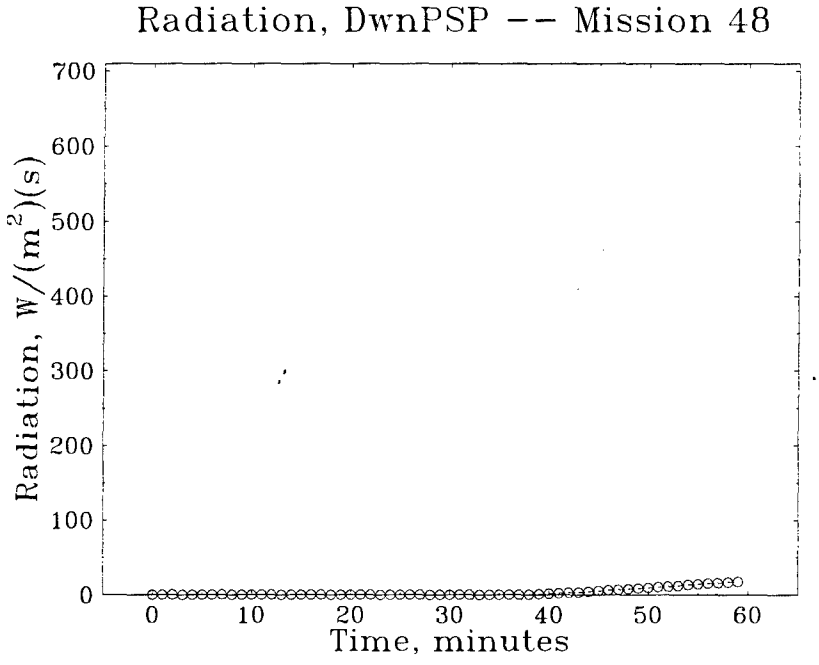

Figure D-7. Downwelling PSP radiation during the first hour of mission 48.

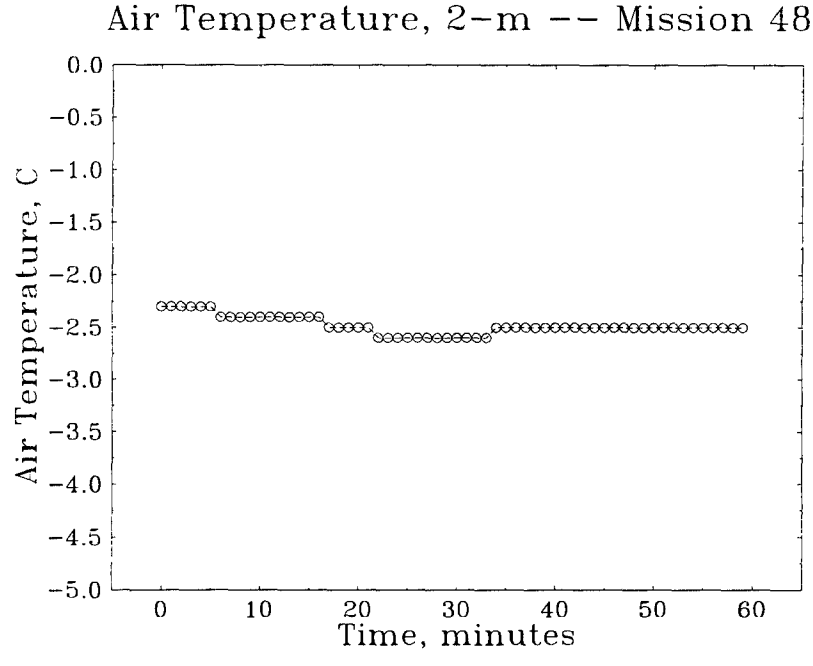

Figure D-8. Air temperature at 2m (AGL) during the first hour of mission 48.

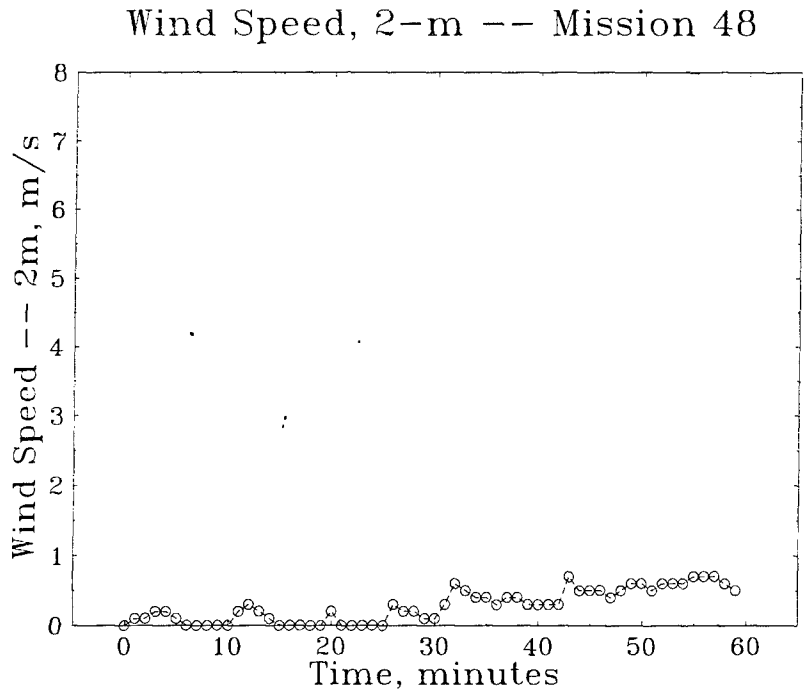

Figure D-9. Wind speed at 2m (AGL) during the first hour of mission 48.

Distribution

	Copies
NASA MARSHAL SPACE FLT CTR ATMOSPHERIC SCIENCES DIV E501 ATTN DR FICHTL HUNTSVILLE AL 35802	1
NASA SPACE FLT CTR ATMOSPHERIC SCIENCES DIV CODE ED 41 1 HUNTSVILLE AL 35812	1
ARMY STRAT DEFNS CMND CSSD SL L ATTN DR LILLY PO BOX 1500 HUNTSVILLE AL 35807-3801	1
ARMY MISSILE CMND AMSMI RD AC AD ATTN DR PETERSON REDSTONE ARSENAL AL 35898-5242	1
ARMY MISSILE CMND AMSMI RD AS SS ATTN MR H F ANDERSON REDSTONE ARSENAL AL 35898-5253	1

ARMY MISSILE CMND 1
AMSMI RD AS SS
ATTN MR B WILLIAMS
REDSTONE ARSENAL AL 35898-5253

ARMY MISSILE CMND 1
AMSMI RD DE SE
ATTN MR GORDON LILL JR
REDSTONE ARSENAL AL 35898-5245

ARMY MISSILE CMND 1
REDSTONE SCI INFO CTR
AMSMI RD CS R DOC
REDSTONE ARSENAL AL 35898-5241

ARMY MISSILE CMND 1
AMSMI
REDSTONE ARSENAL AL 35898-5253

CMD (420000D(C0245)) 1
ATTN DR A SHLANTA
NAVAIRWARCENWPNDIV
1 ADMIN CIR
CHINA LAKE CA 93555-6001

PACIFIC MISSILE TEST CTR 1
GEOPHYSICS DIV
ATTN CODE 3250
POINT MUGU CA 93042-5000

LOCKHEED MIS & SPACE CO 1
ATTN KENNETH R HARDY
ORG 91 01 B 255
3251 HANOVER STREET
PALO ALTO CA 94304-1191

NAVAL OCEAN SYST CTR 1
CODE 54
ATTN DR RICHTER
SAN DIEGO CA 92152-5000

METEOROLOGIST IN CHARGE 1
KWAJALEIN MISSILE RANGE
PO BOX 67
APO SAN FRANCISCO CA 96555

DEPT OF COMMERCE CTR 1
MOUNTAIN ADMINISTRATION
SPPRT CTR LIBRARY R 51
325 S BROADWAY
BOULDER CO 80303

DR HANS J LIEBE 1
NTIA ITS S 3
325 S BROADWAY
BOULDER CO 80303

NCAR LIBRARY SERIALS 1
NATL CTR FOR ATMOS RSCH
PO BOX 3000
BOULDER CO 80307-3000

DEPT OF COMMERCE CTR 1
325 S BROADWAY
BOULDER CO 80303

DAMI POI 1
WASH DC 20310-1067

MIL ASST FOR ENV SCI OFC 1
OF THE UNDERSEC OF DEFNS
FOR RSCH & ENGR R&AT E LS
PENTAGON ROOM 3D129
WASH DC 20301-3080

DEAN RMD 1
ATTN DR GOMEZ
WASH DC 20314

ARMY INFANTRY 1
ATSH CD CS OR
ATTN DR E DUTOIT
FT BENNING GA 30905-5090

AIR WEATHER SERVICE 1
TECH LIBRARY FL4414 3
SCOTT AFB IL 62225-5458

USAFETAC DNE 1
ATTN MR GLAUBER
SCOTT AFB IL 62225-5008

HQ AWS DOO 1 1
SCOTT AFB IL 62225-5008

PHILLIPS LABORATORY 1
PL LYP
ATTN MR CHISHOLM
HANSCOM AFB MA 01731-5000

ATMOSPHERIC SCI DIV 1
GEOPHYSICS DIRCTRT
PHILLIPS LABORATORY
HANSCOM AFB MA 01731-5000

PHILLIPS LABORATORY 1
PL LYP 3
HANSCOM AFB MA 01731-5000

ARMY MATERIEL SYST 1
ANALYSIS ACTIVITY
AMXSY
ATTN MP H COHEN
APG MD 21005-5071

ARMY MATERIEL SYST 1
ANALYSIS ACTIVITY
AMXSY AT
ATTN MR CAMPBELL
APG MD 21005-5071

ARMY MATERIEL SYST 1
ANALYSIS ACTIVITY
AMXSY CR
ATTN MR MARCHET
APG MD 21005-5071

ARL CHEMICAL BIOLOGY 1
NUC EFFECTS DIV
AMSRL SL CO
APG MD 21010-5423

ARMY MATERIEL SYST 1
ANALYSIS ACTIVITY
AMXSY
APG MD 21005-5071

ARMY MATERIEL SYST 1
ANALYSIS ACTIVITY
AMXSY CS
ATTN MR BRADLEY
APG MD 21005-5071

ARMY RESEARCH LABORATORY 1
AMSRL D
2800 POWDER MILL ROAD
ADELPHI MD 20783-1145

ARMY RESEARCH LABORATORY 1
AMSRL OP SD TP
TECHNICAL PUBLISHING
2800 POWDER MILL ROAD
ADELPHI MD 20783-1145

ARMY RESEARCH LABORATORY 1
AMSRL OP CI SD TL
2800 POWDER MILL ROAD
ADELPHI MD 20783-1145

ARMY RESEARCH LABORATORY 1
AMSRL SS SH
ATTN DR SZTANKAY
2800 POWDER MILL ROAD
ADELPHI MD 20783-1145

ARMY RESEARCH LABORATORY 1
AMSRL
2800 POWDER MILL ROAD
ADELPHI MD 20783-1145

NATIONAL SECURITY AGCY W21 1
ATTN DR LONGBOTHUM
9800 SAVAGE ROAD
FT GEORGE G MEADE MD 20755-6000

OIC NAVSWC 1
TECH LIBRARY CODE E 232
SILVER SPRINGS MD 20903-5000

ARMY RSRC OFC 1
ATTN AMXRO GS (DR BACH)
PO BOX 12211
RTP NC 27009

DR JERRY DAVIS 1
NCSU
PO BOX 8208
RALEIGH NC 27650-8208

US ARMY CECRL 1
CECRL GP
ATTN DR DETSCH
HANOVER NH 03755-1290

ARMY ARDEC 1
SMCAR IMI I BLDG 59
DOVER NJ 07806-5000

ARMY SATELLITE COMM AGCY 1
DRCPM SC 3
FT MONMOUTH NJ 07703-5303

ARMY COMMUNICATIONS 1
ELECTR CTR FOR EW RSTA
AMSEL EW D
FT MONMOUTH NJ 07703-5303

ARMY COMMUNICATIONS 1
ELECTR CTR FOR EW RSTA
AMSEL EW MD
FT MONMOUTH NJ 07703-5303

ARMY DUGWAY PROVING GRD 1
STEDP MT DA L 3
DUGWAY UT 84022-5000

ARMY DUGWAY PROVING GRD 1
STEDP MT M
ATTN MR BOWERS
DUGWAY UT 84022-5000

DEPT OF THE AIR FORCE 1
OL A 2D WEATHER SQUAD MAC
HOLLOMAN AFB NM 88330-5000

PL WE 1
KIRTLAND AFB NM 87118-6008

USAF ROME LAB TECH 1
CORRIDOR W STE 262 RL SUL
26 ELECTR PKWY BLD 106
GRIFFISS AFB NY 13441-4514

AFMC DOW 1
WRIGHT PATTERSON AFB OH 0334-5000

ARMY FIELD ARTLLRY SCHOOL 1
ATSF TSM TA
FT SILL OK 73503-5600

NAVAL AIR DEV CTR 1
CODE 5012
ATTN AL SALIK
WARMINISTER PA 18974

ARMY FOREGN SCI TECH CTR 1
CM
220 7TH STREET NE
CHARLOTTESVILLE VA 22901-5396

NAVAL SURFACE WEAPONS CTR 1
CODE G63
DAHLGREN VA 22448-5000

ARMY OEC 1
CSTE EFS
PARK CENTER IV
4501 FORD AVE
ALEXANDRIA VA 22302-1458

ARMY CORPS OF ENGRS 1
ENGR TOPOGRAPHICS LAB
ETL GS LB
FT BELVOIR VA 22060

ARMY TOPO ENGR CTR 1
CETEC ZC 1
FT BELVOIR VA 22060-5546

SCI AND TECHNOLOGY 1
101 RESEARCH DRIVE
HAMPTON VA 23666-1340

ARMY NUCLEAR CML AGCY 1
MONA ZB BLDG 2073
SPRINGFIELD VA 22150-3198

USATRADOC 1
ATCD FA
FT MONROE VA 23651-5170

ARMY TRADOC ANALYSIS CTR 1
ATRC WSS R
WSMR NM 88002-5502

ARMY RESEARCH LABORATORY 1
AMSRL BE S
BATTLEFIELD ENVIR DIR
WSMR NM 88002-5501

ARMY RESEARCH LABORATORY 1
AMSRL BE E
BATTLEFIELD ENVIR DIR
WSMR NM 88002-5501

ARMY RESEARCH LABORATORY 1
AMSRL BE W
BATTLEFIELD ENVIR DIR
WSMR NM 88002-5501

DTIC
8725 JOHN J. KINGMAN RD
STE 0944 1
FT BELVOIR VA 22060-6218

ARMY MISSILE CMND 1
AMSMI
REDSTONE ARSENAL
AL 35898-5243

USATRADOC 1
ATCD FA
FT MONROE VA 23651-5170

WSMR TECH LIBRARY BR 1
STEWS IM IT
WSMR NM 88001

SWOE JT & E PROGRAM OFFICE
ATTN DR JP WELSH 5
US ARMY COLD REGIONS RESEARCH LAB
72 LYME ROAD
HANOVER NH 03755

US ARMY RESEARCH LABORATORY ATTN MAX BLEIWEISS AMSRL IS EW WSMR NM 88002	20
Record Copy	1
TOTAL	98